Journal of Sol-Gel Science and Technology (2021) 98:1–23
https://doi.org/10.1007/s10971-021-05504-2

INVITED REVIEW: CHARACTERIZATION METHODS OF SOL-GEL AND HYBRID MATERIALS

The ellipsometry versatility in the study of sol-gel films

Mariuca Gartner[1] · Mihai Stoica[1] · Madalina Nicolescu[1] · Hermine Stroescu[1]

Received: 21 September 2020 / Revised: 2 February 2021 / Accepted: 9 February 2021 / Published online: 8 March 2021

Abstract

Spectroscopic ellipsometry (SE) with its fast, precise, non-destructive and non-contact nature, working both ex situ and in situ, is the ideal characterization tool for thin films in terms of optical, struactural and electrical information obtained over wide application domains. The review aims to prove the versatility of such a powerful technique, starting with the basic knowledge of the ellipsometry, extending the application field from UV–vis-NIR to VUV and IR domains, and then advancing to the analyses of porosity, anisotropy, surface mapping and bowing parameter. The examples shown in this review illustrate the complementarity of ellipsometry with other characterization techniques, highlighting the sensitivity and the quality of the results especially in the domain of the sol–gel films.

Graphical Abstract

Spectroscopic ellipsometry: all-in-one technique for a variety of material characteristics.

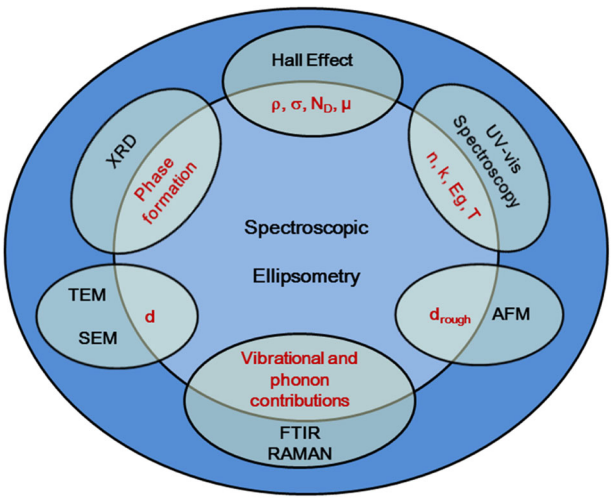

Keywords Ellipsometry · Sol–gel · Thin films · Optical properties

✉ Madalina Nicolescu
mnicolescu@icf.ro

✉ Hermine Stroescu
hermine25@yahoo.com

[1] Institute of Physical Chemistry "Ilie Murgulescu", Romanian Academy, 202 Splaiul Independentei, 060021 Bucharest, Romania

Highlights

- Versatility of the ellipsometry is illustrated on sol–gel films.
- SE, all-in-one technique, for the study of a variety of material characteristics.
- Possibility to obtain optical constants on a large spectral range (0.193–33 μm) is shown.
- Suitability of SE for anisotropy, porosity, vibrational, mapping, and bowing parameter analysis is presented.
- Detailed complementary information is obtained combining SE with other characterization methods.

1 Introduction

The light is a fascinating subject of study, even the ancient Greeks were intrigued by its nature. But only later in the 1600s there was a real progress in the understanding of the mathematical and physical principles of the light. This led to the study of the thin films in the early 1900s by employment of classical optics. The term "ellipsometry" was established only in the mid-1900s. The founder of the basic principles of ellipsometry is Paul Drude, which derived in 1887 the equations of ellipsometry, a remarkable achievement if we think that these equations are still used today. The model which describes the optical properties of metals is named after him. Despite its simplicity and its accuracy, ellipsometry was not so popular until 1970s, when ellipsometers moved from manually operated and hence very time-consuming to automate instruments. The first complete automation of spectroscopic ellipsometry (SE) was realized by Aspnes et al. [1] in 1975, followed in 1984 by the first real-time monitoring with a spectroscopic ellipsometer achieved by Müller and Farmer [2]. Development of computer technology led to an increase in the number of measurement data and degree of precision. It was just a matter of time until ellipsometry became the most essential characterization technique for coatings. With every development step ellipsometers led to a shorter measuring time and more precise analysis data, as the real-time instrument developed in 1990 by Kim et al. [3], which utilizes a photodiode array (PDA) detector, that allows simultaneous measurement of light intensities at multi-wavelengths.

Nowadays, application of ellipsometry in various domains is a current practice. From microelectronics to medicine and biology, ellipsometry is focused on improving accuracy and sensitivity, and on corroborating with complementary data obtained from multiple techniques [4].

Ellipsometry is an optical measurement technique that characterizes light reflection or transmission from a sample. The name "*ellipsometry*" is given by the polarized light which becomes "elliptical" upon light reflection. By measuring the change in polarization of the reflected light, ellipsometry determines the amplitude ratio (Ψ) and phase shift (Δ) between *p*- (parallel) and *s*- (perpendicular) polarized light waves. The values of these two ellipsometric parameters are measured in the ultraviolet, visible and infrared spectral ranges.

Ellipsometry is a non-destructive and non-contact measurement technique, which requires two conditions in order to perform a successful measurement on any sample, namely: (1) surface roughness of samples should be <30% of a measurement wavelength, otherwise the scattering occurs and the intensity of the reflected light will be reduced, making harder the determination of the polarization state, and (2) depending on the optical constants of samples, the incidence angles must be chosen in order to maximize the measurement sensitivity.

From the absolute values of Ψ and Δ is difficult to give an interpretation of measurement results, thus, construction of an optical model is needed for data analysis and to determine the physical properties of a sample. Ellipsometry allows the evaluation of the refractive index n and extinction coefficient k of the material under study, and the complex refractive index defined by $\tilde{N} \equiv n - ik$ is determined. The complex dielectric constant $\tilde{\varepsilon}$ and absorption coefficient α can also be obtained from the following relations: $\tilde{\varepsilon} = \tilde{N}^2$ and$\alpha = \frac{4\pi k}{\lambda}$, respectively.

Measurements carried out in different parts of the spectral domain give specific optical characteristics. In the UV–visible region, ellipsometry can characterize the interband transitions and make an estimation of the bandgap (Eg) from the variation of α with $h\upsilon$, where h is the Planck's constant, and υ is the light frequency. Moreover, from the spectral analysis of the optical constants, the alloy composition, crystal grain size and phase structure can be determined.

In the infrared spectral range, properties like lattice vibration modes (LO and TO phonon) can be determined by ellipsometry [5]. Determination of electrical properties, including carrier concentration, carrier mobility and conductivity, and local atomic structures is also possible [6].

The ellipsometric measurements can be performed not only in air but also in situ (vacuum [7], liquid [8], or in a controlled atmosphere [9–13]); they can be static or dynamic (in real time). In the last mode, the ellipsometry can be used as a control technique of different processes [14–19].

Like any other method, the ellipsometry has its advantages and drawbacks, which are summarized in Table 1. The high sensitivity of ~0.1 Å [20] of ellipsometric measurements makes this technique to be very useful and precise in determining thin film thickness, surface and interfacial roughness. Its sensitivity refers also to the optical (dielectric) constants of the layer and hence to the bandgap energy, to the uniformity of the layer, to the anisotropy, porosity and density of the layer, to the conductivity-resistivity and

Table 1 Advantages and disadvantages of spectroscopic ellipsometry

Advantages	Disadvantages
Non-destructive and non-contact technique	Building an optical model to analyze the experimental data
Extremely precise and fast	Data analysis could be time consuming
Monitoring in real-time, in situ (vacuum, liquid)	The spatial resolution is low
Application on wide domains Transmittance and mapping measurements	Materials with low absorption coefficients ($\alpha < 100\,cm^{-1}$) are difficult to be characterized

to molecular vibrations, to the growth or etching kinetics in real-time monitoring, and to any other physical effect that induces changes in the optical properties of the materials.

Spectroscopic ellipsometry finds applications in a wide area of domains, mentioning semiconductor industry (substrates, thin films, lithography, gate dielectrics) [21, 22], chemistry (self-assembled monolayers, polymer films, proteins) [23, 24], optical coatings (high and low dielectrics) [25, 26], displays (TCOs, TFT films, organic LEDs) [27] and data storage (phase change media, magneto-optic layers) [28, 29].

The use of spectroscopic ellipsometry in areas of biology for the study of organic layers was also reported, including applications such as protein monolayer spectroscopy, in situ monitoring of protein adsorption on planar surfaces and in porous layers and ellipsometric imaging for determination of thickness distributions [30], in the study of chiral nanocrystalline cellulose films [31].

For biological studies were developed ellipsometers like FPE (fixed polarizer ellipsometer) [32] and MIE (microscopic imaging ellipsometry) [33], with different measurement capabilities.

Many approaches were proposed for maximizing the measurement spot size and for optimizing the measurement time in order to achieve more reliable results in a short time for conventional ellipsometers, including a snap-shot ellipsometric configuration by Lee et al. [34]. The co-axial optical structure allows high magnification (100×) objective lens, which lead to a spot size of a 62 µm and coupled with snap-shot ellipsometry lead to real-time measurements with high precision over various thickness values of samples, thus solving the issues of large spot size and long measurement time of conventional ellipsometry, maintaining the accuracy.

Recent papers on sol–gel film ellipsometry underline the influence of precursor concentrations [35], pH of the sol [36], annealing procedure (type and time) [37] and dopants [38] on their optical properties.

Among the methods used in the characterization of nanomaterials, ellipsometry has proven by its versatility and its sensitivity to be the right choice for the complex characterization of thin films [39].

In the review are exemplified with predilection three oxidic materials: *ZnO, TiO_2 and ITO* which are among the most studied semiconductor materials due to their multifunctional properties different from other transition metal oxides or III-V, II-VI semiconductors. They have similar properties, like wide bandgap, good optical transparency, high electrical conductivity, antibacterial behavior, thus they can be used in a huge number of applications as: photocatalysts, gas sensors, wastewater treatment, film transistors, liquid crystal displays, LEDs and OLEDs, solar cells, photovoltaics, flat panel displays, smart windows, antistatic coatings and many more. They can be easily prepared as thin film not only by physical methods but also by less expensive chemical ones. All of them can be doped or even co-doped, resulting materials with improved properties and can be prepared in the shape of nanoparticles, nanowires, nanorods and other 2D dimensional shapes, presenting unique features.

NOTE: The following sections of the review will guide the reader through the theory, principles and applications of spectroscopic ellipsometry (SE). The main issues to which the review presents solutions are: what is ellipsometry and how it can be used in the investigation of the sol–gel thin films;what are the physical properties measured by SE; what is an optical model and how it can be used to simulate a real sample; *what are the method limitations and how can we get additional information from extreme parts of the spectral regions; how can we apply ellipsometry to non-ideal samples and how to get complex features out of ellipsometric analysis. Finally, the review aims at highlighting the versatility and sensitivity of SE by the selected examples in connection with the sol–gel deposition method.*

2 Theory

2.1 Basic knowledge of the ellipsometry theory

Ellipsometry measures the change of the polarization of the light after reflection on a surface. In general, the light after the reflection on a surface is elliptically polarized, but for a special position of the analyzer (Δ), the reflected light is linearly polarized. In this case, the polarizer can extinguish the light at a certain orientation (Ψ) (Fig. 1). The electric

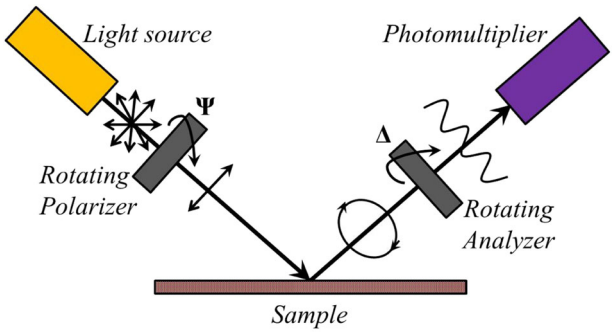

Fig. 1 Schematic representation of an Ellipsometer

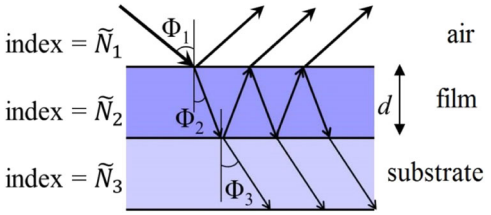

Fig. 2 Reflection and refraction of the incident light in a film deposited on a substrate

vector of both the incident and reflected light can be decomposed in parallel (p) and perpendicular (s) components on the incidence plane. The ratios of the reflected and incident electric components, parallel and normal to the incidence plane, represent the Fresnel (Rp, Rs) coefficients, which contain information about material and layer structure.

The Fresnel coefficients are linked to the angles Ψ and Δ by the fundamental equation of the ellipsometry:

$$\rho = \tan(\Psi)e^{i\Delta} = \frac{R_p}{R_s} \tag{1}$$

In the case of a film, Fresnel coefficients contain information about all three media (Fig. 2):

- medium 1 is in general air (or vacuum or a liquid)
- medium 2 is the film with a complex refractive index $\tilde{N} = n - ik$, and a thickness d
- medium 3 is the substrate

Φ_1 and Φ_2 are incident and refracted angles, respectively. where:

$$R_p = \frac{R_p^{12} + R_p^{23}\exp(-i2\beta)}{1 + R_p^{12}R_p^{23}\exp(-i2\beta)}\, R_s = \frac{R_s^{12} + R_s^{23}\exp(-i2\beta)}{1 + R_s^{12}R_s^{23}\exp(-i2\beta)}\ \textit{oscillating in}\ \beta = \frac{\pi d N_2 \cos\phi_2}{\lambda} \tag{2}$$

β being the film phase thickness

An ellipsometric experiment consists of the following steps:

- the measurement of Ψ and Δ parameters
- building an optical model
- calculating the response from the model
- fitting the calculated data with the experimental measurements, using regression analysis
- choosing the model to match the measurements. The best fit is obtained when the Mean Squared Error-MSE (which quantifies the difference between experimental and model-generated data) has the smallest value corresponding to the best fit.

$$MSE = \frac{1}{2N - M}\sum_{i=1}^{N}\left[\left(\frac{\Psi_i^{mod} - \Psi_i^{exp}}{\sigma_{\Psi,i}^{exp}}\right)^2 + \left(\frac{\Delta_i^{mod} - \Delta_i^{exp}}{\sigma_{\Delta,i}^{exp}}\right)^2\right] = \frac{1}{2N - M}\chi^2 \tag{3}$$

where:

N is the number of (Ψ, Δ) pairs

M is the number of variable parameters in the model

σ are the standard deviations on the experimental data points

- from the best fit, n, k and d are obtained

To be consistent, the ellipsometric equations must obey the Kramers–Kronig (KK) rule [20], where the real and imaginary part of the dielectric constants (ε_1 and ε_2) depend on each other.

2.2 Some important models in ellipsometric characterization of sol–gel films

From an ellipsometric measurement results only two values, Ψ and Δ, which are insufficient to obtain all physical parameters of the sample under study, so a model based on regression analysis must be used.

To fit the ellipsometric experimental spectra are used either the tabulated optical constants of materials stored in the fitting software or different models based on optical oscillators. Since generally the optical constants of a material depend on the preparation method, a fit model based on oscillators is more adequate. In the simulating data a model needs to be as close to the real sample as possible.

In the simplest case of transparent materials, one can use Cauchy equation [40], which describes well the dispersion for materials which are essentially non-absorbing over the measured spectral range. The *Cauchy* relation is most effective when curve fitting a normal dispersion (n decreasing with wavelength). The Cauchy equation for the refractive index is given by

$$n(\lambda) = A_n + \frac{B_n}{\lambda^2} + \frac{C_n}{\lambda^4} \tag{4}$$

where A_n, B_n, C_n are called *Cauchy parameters*. The "A_n" term is a constant and describes the long-wavelength

asymptotic index value, while the "B_n" and "C_n" are the dispersion terms that add upward slope to the index value as wavelengths become shorter (B_n and $C_n \geq 0$).

Since the Cauchy equation involves no absorption, it is not Kramers–Kronig consistent. In the IR range, the absorption bands are due to molecular vibrations and in the UV due to electronic vibrations, while in the visible region the occasional absorptions are for organic films, for example. For the materials which are slightly absorbing in the UV, a convenient representation of the extinction coefficient (not zero) is given by the Urbach equation [41], namely

$$k(\lambda) = A_k e^{B(E-Eb)} \tag{5}$$

where A_k is the amplitude and B is the exponent, both being called *Urbach parameters*. This exponential function represents an Urbach absorption tail. The limitations of the Cauchy and Urbach parameterization of the optical response are clearly seen for strongly absorbing materials, like thin metal films (more details in the paragraph 4.4)

In the case of small particles of one material embedded in a matrix of the host material is suitable to use Effective Medium Approximation (EMA) [42]. In this case, the assumptions are

- each material retains bulk-like optical properties (grain size large enough to ignore quantum size effects),
- sufficient mixing over a macroscopic area (grain size small enough to appear homogenous compared to the wavelength of light—no scattering).
- There are different types of equations based on Effective Medium Approximation, such as:
- Lorentz–Lorenz (LL) where the host is air,
- Maxwell–Garnett (MG) where the host is not air and describes the inclusion of small volume fraction in a host material,
- Bruggeman where the host is the effective medium.

All these approximations use the same equation with different "host" material

$$\frac{\varepsilon_{eff} - \varepsilon_h}{\varepsilon_{eff} + 2\varepsilon_h} = f_1 \frac{\varepsilon_1 - \varepsilon_h}{\varepsilon_1 + 2\varepsilon_h} + f_2 \frac{\varepsilon_2 - \varepsilon_h}{\varepsilon_2 + 2\varepsilon_h} + \ldots \tag{6}$$

where, $\boldsymbol{\varepsilon}$ is the complex dielectric function for: effective medium (*eff*), host (*h*), and constituent materials (*1, 2*, …); f_1 and f_2 are volume fractions of each constituent.

This model is particularly useful to simulate surface roughness, intermix layers, gradient layers, or doped layers [12, 43–48].

For more complex films, oscillator models are more suitable because they can describe optical constants in transparent and absorbing regions in the same time, maintains Kramers–Kroning consistency and used a reduced number of "fit" parameters.

For a normal dispersion, the refractive index increases toward higher frequencies when there is no absorption. For an anomalous dispersion, absorption causes changes in real part (n).

Different type of absorptions matches different oscillators:

- organic and dielectrics: UV resonant absorptions—Gaussian [49], Tauc-Lorentz [50]
- semiconductors: direct bandgap—Psemi-E0 [51]

  indirect gap / amorphous—Tauc-Lorentz or Cody-Lorentz [50]
  higher energy transitions—Gaussian or PSEMI [51]

- metals: free carrier absorption—Drude [52, 53], Lorentz [54, 55], Harmonic [56]

Lorentz oscillator is a classic harmonic oscillator, with long absorption tails which can cause unwanted absorption in transparent regions. The model is best suited for phonons or metals, where absorption exists over all wavelengths.

$$\tilde{\varepsilon} = \frac{AE_0}{E_0^2 - E^2 - i\gamma E} \tag{7}$$

where, A is the amplitude, E_0 is the center energy, γ is the broadening of the oscillator, while E is the photon energy in eV.

Gaussian oscillator is an oscillator with shorter absorption tails than Lorentz—the absorption drops rapidly to zero; used for materials with band gaps, infrared absorptions in amorphous materials, multiple UV absorptions in amorphous materials.

$$\varepsilon_2 = A_n e^{-\left(\frac{E-E_n}{Br_n}\right)^2} + A_n e^{-\left(\frac{E+E_n}{Br_n}\right)^2} \tag{8}$$

$$\varepsilon_1 = \frac{2}{\pi} P \int_0^\infty \frac{\xi \varepsilon_{n2}(\xi)}{\xi^2 - E^2} d\xi \tag{9}$$

Drude oscillator is a Lorentz oscillator with $E_0 = 0$; it describes free carries because of no restoring force; used for metals, doped semiconductors and conductive dielectrics; method for non-contact measurement of resistivity, thus *obtaining directly the electrical parameters without Hall measurements*.

$$\tilde{\varepsilon} = -\frac{A}{E^2 + i\gamma E} \tag{10}$$

Tauc-Lorentz oscillator includes bandgap energy (E_g), with no absorption allowed below gap energy, good for amorphous semiconductor and other UV absorptions.

Another combination of oscillators used in semiconductor-type materials characterization is **Tauc-Lorentz** (which describes the absorption in UV) and **Drude** (which describes the effect of the electric charge carriers on the dielectric function when passing from the visible to the infrared wavelength range) oscillators. The carrier concentration (N_D), the mobility (μ), resistivity (ρ) and the optical conductivity (σ) were determined using the equation:

$$\rho = \frac{\gamma}{\varepsilon_0 \omega_p^2} \rightarrow \rho = \frac{m^*}{N_D q^2 \tau} = \frac{1}{q \mu N_D} \rightarrow \sigma = e N_D \mu = 1/\rho \tag{11}$$

where: ρ—optical resistivity (Ω cm)

γ—relaxation rate or damping coefficient of free carriers (1/s)

ω_p—plasma frequency (1/s)

τ—electron scattering time (sec) ($\tau = 1/\gamma$)

m^*—effective electron mass (Kg)

N_D—carrier concentration (cm^{-3})

μ—carrier mobility (cm^2/Vs)

ε_o—vacuum dielectric constant (F/m)

q—electron charge (C)

σ—optical conductivity (1/ Ω cm)

Optical absorptions in a material occur in different parts of the light spectrum, having different shapes, depending on the cause that generates them, like the free carriers (mostly in IR), electronic transitions (in UV–vis–NIR), molecular vibrations and lattice vibrations (in mid-IR). To describe the spectral behavior of the optical functions for the absorbing materials, one or more oscillators are usually used.

The General Oscillator Layer (shortly "GenOsc") models the dielectric function of a film or substrate as a linear summation of real or complex terms, each of them being a function of wavelength (nm) [wavenumber (cm^{-1}) or photon energy (eV)]. This model was developed in the WVASE® software, to simplify the analysis of the optical constants. The GenOsc model allows the user to choose more oscillators (Lorentz, Drude, Gauss, Tauc–Lorentz, Gauss–Lorentz, Cody-Lorentz, etc.) to simulate more accurately the dielectric functions of a material [57]. This formalism uses K–K consistent oscillator equations.

The multitude of oscillator types used to fit directly the reference dielectric functions, which allows the user to build models fast and accurate, makes the GenOsc a powerful and flexible model.

Several other important oscillators used in the ellipsometric simulations are: *harmonic* (classic harmonic oscillator), *ionic* (phonon absorption for IR), *TOLO* [58] (optical phonon absorption with both TO—transverse mode and LO—longitudinal mode broadening), *CPPB* [59] (Critical Point Parabolic Band): oscillator for semiconductors), *CPM* [60] (Adachi models for critical point functions), Tanguy [61] (provides an analytical expression of Wannier excitons), *Herzinger-Johs "P-Semi"* (4 connected functions to model each peak) [51].

3 Versatility of the ellipsometry

3.1 The correspondence between the results obtained by SE and other techniques

In this chapter the high versatility of the spectroscopic ellipsometry is emphasized, by drawing a parallel between SE on the one hand and several different methods on the other hand [62], in determining film characteristics such as (Fig. 3):

(a) optical constants (n, k), optical band gap (E_g) and transmission (T) of the films which are usually determined by UV–vis spectroscopy and optical transmission,
(b) film thickness (d) which is normally measured by Scanning Electron Microscopy (SEM) or Transmission Electron Microscopy (TEM) analyses,
(c) roughness (d_{rough}) determined mainly by Atomic Force Measurements (AFM),
(d) crystallization state signaled by X-ray diffraction (XRD) technique,
(e) information on the chemical components existing in the film, which is the domain of Fourier Transform Infrared Spectroscopy (FTIR),
(f) vibrational properties obtained mainly by Raman Spectroscopy,

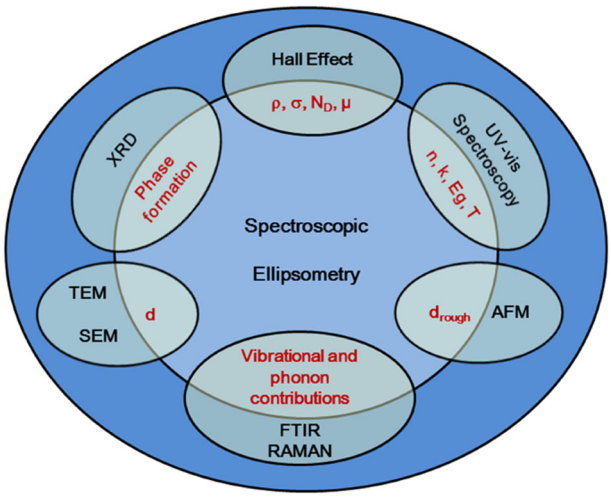

Fig. 3 Spectroscopic ellipsometry: all-in-one technique for a variety of material characteristics

(g) resistivity (ρ), conductivity (σ), carrier concentration (N_D) and mobility (μ) which are usually obtained from Hall measurements.

The following examples illustrate the correspondence between the results obtained by SE and other techniques.

3.1.1 SE vs optical transmission

The refractive index can be obtained by SE, as through optical transmission [63] with the same results. Such an example is offered by Stoica et al.[64]. who modeled sol–gel nanocrystalline ITO multilayer films by both methods. The modeling of SE spectra was performed using a multilayer and multicomponent Bruggemann effective medium approximation (BEMA) as well as a dispersion equation combining the Drude theory, with a double Drude–Lorentzian oscillator (DL) model. As can be seen from Fig. 4, the two estimations agree well.

3.1.2 SE vs TEM

The thickness obtained by Cross-Sectional Transmission Electron Microscopy—XTEM (a very expensive method) can be obtained also by SE (an inexpensive method) as showed by Covei et al.[65].. In the UV–vis ellipsometric data analysis of the Nb doped TiO_2 sol–gel film with 10 layers, the "General Oscillator" model was applied, considering one Tauc-Lorentz oscillator (see Section 1.2). The surface roughness was taken into account, considering the top layer consisting of 50% voids and 50% film material within the effective medium approximation model (see Section 1.2), even though the films are very smooth. The thickness obtained from the best fit (Fig. 5a) was 339.9 nm and agrees well with the thickness obtained by XTEM analysis, 340 nm (Fig. 5b).

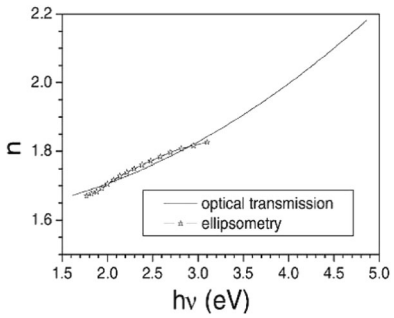

Fig. 4 The comparison of the refractive indices obtained by optical transmission and ellipsometry for four-layer sol–gel ITO film [Reproduced from reference [64] with the permission of Elsevier]

The film thicknesses obtained from TEM investigations are in good agreement with SE results, also in the paper of Zaharescu et al.[67]. who study the change of the sol–gel HfO_2 thin film properties function of used precursor (hafnium ethoxide, hafnium 2,4-pentadionate and hafnium chloride).

3.1.3 SE vs XRD

The formation of anatase (A) and rutile (R) phases in thin $TiO_2(Ni^{2+})$ films (deposited by sol–gel on Al thin film/glass and Si substrates) were observed in parallel by XRD and ellipsometry methods. The as-deposited films were amorphous, but after thermal treatment (TT) they react differently [68]. The $TiO_2(Ni^{2+})$ films (30 nm thick) deposited on Al substrate after 1 h TT at 300 °C crystallize in the anatase form which can be visualized in SE spectrum at 370 nm (Fig. 6a), together with the transfer charge (TC) band from 320 nm. It is known that in the case of very thin films the anatase is formed after treatment at low temperature. For the same type of film deposited on Si substrate (Fig. 6b) and higher TT (700 °C), besides the anatase, the rutile band also appears at 377 nm. The veracity of these assignations is proved by the XRD analysis (Fig. 6b inset figure).

Moreover, a shift of charge transfer adsorption band (TC) from 350 nm (glass) to 330 nm (Si) and 320 nm (Al) is also observed in the ellipsometric spectra of $TiO_2(Ni^{2+})$

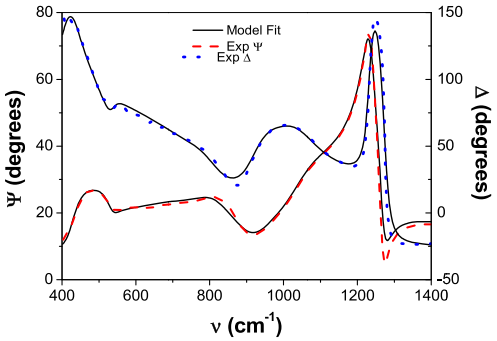

(a)

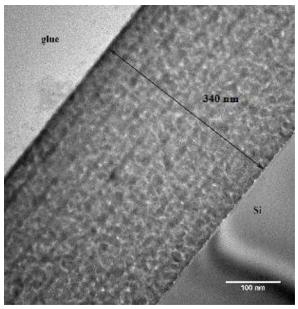

(b)

Fig. 5 Nb doped TiO_2 sol–gel film with 10 layers: **a** Experimental and simulated spectra of the Ψ and Δ ellipsometric parameters modeled with the Tauc-Lorentz model, **b** XTEM image [Reproduced from references (**a**) [65] and (**b**) [66] with the permission of Elsevier]

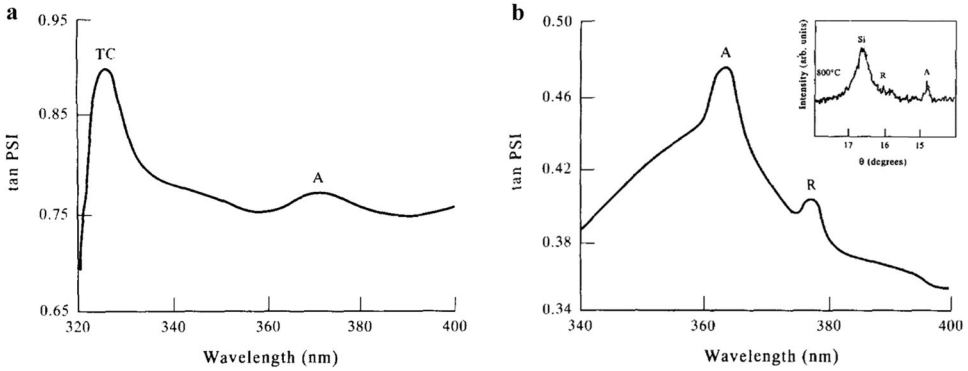

Fig. 6 **a** SE spectrum of Ψ parameter of $TiO_2(Ni^{2+})$/**Al/glass**, TT 1 h at 300 °C. **b** SE spectrum of Ψ parameter of $TiO_2(Ni^{2+})$ /**Si**, TT 1 h at 700 °C. *Inset: XRD difractogram.* Reproduced from reference [68] with the permission of Elsevier

Table 2 Comparison of the electrical parameters obtained by SE and Hall for the sol–gel ITO (15 layers) films

Substrate	N_D (10^{20} cm^{-3})		μ (cm^2/Vs)		ρ (10^2Ω cm)		σ (Ω cm)$^{-1}$	
	SE	Hall	SE	Hall	SE	Hall	SE	Hall
Glass	1.61	3.71	2.76	1.05	1.41	1.60	71.12	80.38
Glass/SiO2	1.48	1.78	2.10	1.21	1.99	2.90	50.25	34.50

deposited on Al, Si and glass substrates, due mainly to the lowering of the film thickness and the increase in the refractive index [68].

3.1.4 SE vs FTIR

Vibrational bands of film components can be evidenced by FTIR as well as by IRSE. A good example is that of sol–gel ITO films with 15 layers, deposited on Si where the vibrational bands were determined by IRSE (see in details in Section 3.2).

3.1.5 SE vs Hall

Electrical properties can be determined by SE as well as by Hall measurements. An example is the sol–gel ITO films with 15 layers deposited on glass and SiO_2/glass [69] which was modeled by a combination of Tauc -Lorentz (to describe the absorption in UV) and Drude (to describe the effect of the electric charge carriers on the dielectric function when passing from the visible to the infrared wavelength range) oscillators (see Section 1.2).

As can be seen in Table 2, the values of the electrical parameters obtained by Hall measurements validate, as order of magnitude, the ellipsometric results.

In terms of absolute values, the results are not always very close. A possible explanation could be that the ellipsometry is an indirect technique which requires data modeling (the dielectric function using the Tauc-Lorentz and Drude oscillator models), while the electrical parameters values are obtained directly through Hall measurements [70–72].

Despite the inherent differences, comparable values for the properties of interest could be obtained. SE method proves to be useful in this case to obtain a large view of the electrical parameters.

In conclusion, the two ellipsometric parameters (Ψ, Δ) were measured in a wide spectral range (0.19–33 μm) and were fitted by combining the Gaussian, Tauc-Lorentz, Lorentz and Drude oscillators to obtain the complex optical constants (e.g. complex refractive index, complex dielectric function). With these values were further estimated the thickness, free-carrier contribution and vibration modes. The frequencies TO and LO modes are related through the Lyddane–Sachs–Teller (LST) relation [73]:

$$\frac{\omega_{LO}^2}{\omega_{TO}^2} = \frac{\varepsilon_0}{\varepsilon_\infty} \tag{12}$$

Where: ω_{Lo} — the longitudinal vibration frequency (cm^{-1})
ω_{To} — the transverse vibration frequency (cm^{-1})
ε_0 — the low-frequency dielectric constant
ε_∞ — the high-frequency dielectric constant

The results presented in this study show that Spectroscopic Ellipsometry is complementary with other techniques (Fig. 3) and their combination provides a better understanding of the experimental data.

3.2 Information obtained directly from ellipsometric spectra, prior to the data modeling

3.2.1 Visualization of different bands was already described above (Section 2.1.3) in UV spectral range [68]

3.2.1.1 Estimation of the film's thickness Interference oscillations of the spectra of the ellipsometric parameters Ψ and Δ are affected by the thickness (d) and refractive index (n) of the film. For the films with the same material characteristics, but having different thicknesses, the parameter d can be estimated from ellipsometric spectra by counting the numbers of oscillations. As the thickness increases, the number of oscillations grows. At the same time, the maxima of thicker film

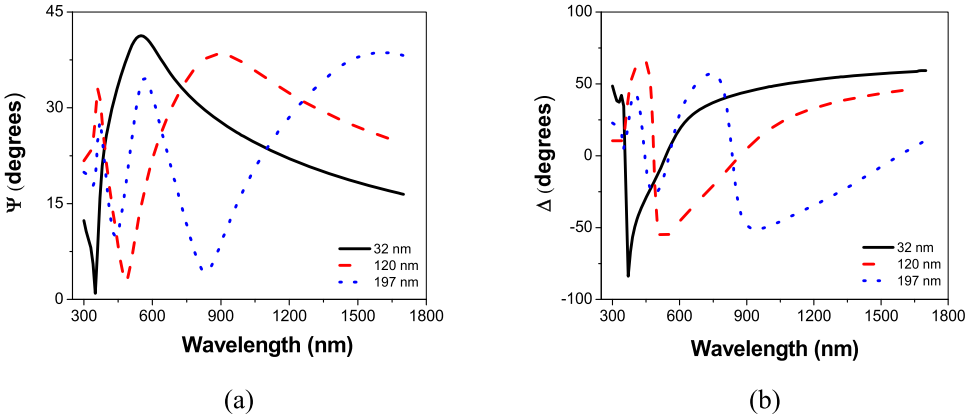

Fig. 7 Thickness evolution visualized on experimental ellipsometric spectra (**a**) Ψ and (**b**) Δ of ZIRO film

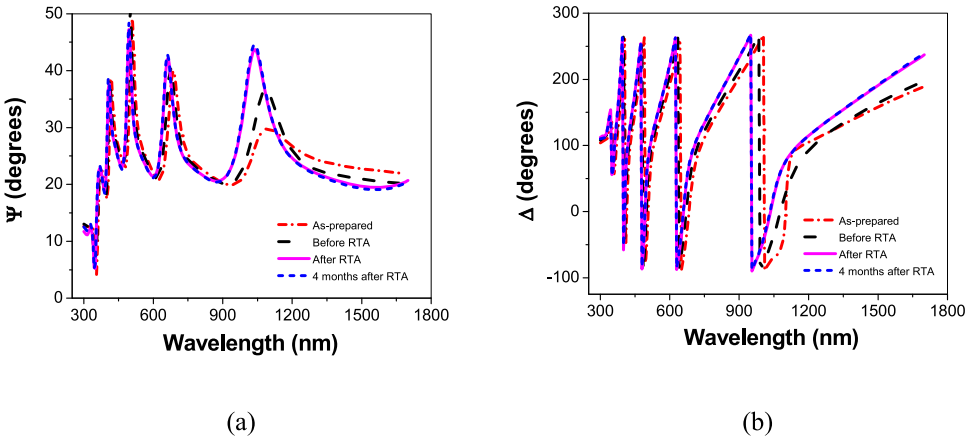

Fig. 8 Experimental ellipsometric spectra (**a**) Ψ and (**b**) Δ presented comparatively for sputtered ITO/Si(100) film before and after the RTA treatment (1 min, 400 °C) [Reproduced from reference [75] with the permission of Elsevier]

shift to higher wavelengths. One example can be seen in Fig. 7 representing the oscillations of Ψ parameter with the thickness of oxide ternary alloys Zn–Ir–O (ZIRO) [74].

3.2.2 Checking the stabilization of the films

One of the most important ellipsometric applications for film technology is the monitoring of the surface stability of the films. The changes of the film surface can be viewed directly by tracking the evolution of the ellipsometric parameter (Ψ and Δ) spectra.

A comparison between the experimental ellipsometric spectra taken on the as-deposited film, the annealed one and after some months can offer us information about the changes happening on the film surface. The efficiency of a *rapid thermal annealing treatment* (RTA) for 1 min up to 400 °C in N_2 atmosphere on an ITO film deposited by reactive sputtering on Si(100) substrate is shown by Stroescu et al. [75]. They observed that the ellipsometric spectra taken after RTA treatment remain practically unchanged (Fig. 8—the measurements are performed in the same area) even after 4 months. This result proves that the RTA treatment stabilized well the sample surface.

In comparison with the RTA treatment for 1 min up to 400 °C, a *normal thermal annealing treatment* (NTA) for 1 h at 400 °C in nitrogen atmosphere is not so efficient. In the case of ITO films deposited by sol–gel method on Si(111) substrate (Fig. 9—will be published), the stabilization of the film by NTA was less efficient than by immersion of the film for 24 hours in an alcoholic solution containing 2 mM 1-Octadecanethiol/$CH_3(CH_2)_{17}SH$. The ellipsometric spectra of Ψ parameter (before and after stabilization treatment with 1-Octadecanethiol) are almost unchanged (see Fig. 9), while the Ψ spectra for the film after a normal thermal annealing treatment (1 h, 400 °C) shifted to smaller wavelengths, thus means that the film thickness was changed.

In conclusion, in this case a Thiol protective surface layer is more efficient for the stabilization of the surface and for a longer time than the normal thermal annealing treatment in nitrogen.

3.2.3 Optical phonon contribution

In the usual way, $E_1(TO)$ frequency mode can be visualized in the spectrum of the imaginary part of dielectric constant (ε_2) and $A_1(LO)$ in the dielectric loss functions $\mathrm{Im}(-\varepsilon^{-1})$ of

IR ellipsometric spectra (IRSE), but they can be also visualized directly in the ellipsometric spectra of Ψ and Δ parameters, which is a substantial advantage. Such an example is offered by Nicolescu et al.[76]. on ZnO:N films deposited by reactive sputtering in a 10% nitrogen atmosphere on Si(100) substrate. The authors show comparatively the assignations of E_1(TO) and A_1(LO) modes directly from the spectra of Ψ and Δ (Fig.10a, b) and from dielectric constants spectra (Fig. 10c, d).

This advantage of the ellipsometry is shown also by Bundesmann [77] on amorphous hafnium aluminate film deposited by metal organic chemical vapor deposition on silicon substrate; by Ashkenov et al. [78] on ZnO films deposited by pulsed-laser deposition (PLD) on *c*-plane sapphire substrates and by Kang [79] on PZT films grown on platinized silicon substrates by using the sol–gel method and on (0001) sapphire by using radio-frequency sputtering deposition.

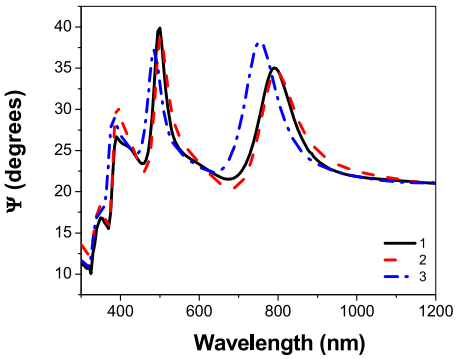

Fig. 9 The stability monitoring of the sol–gel ITO/Si(111) film: (1) as prepared, (2) treated with Thiol, (3) after NTA (1 h, 400^{0}C)

4 Extensions of the basic ellipsometry

4.1 Vacuum UV Ellipsometry (VUV)

A spectral region of high interest for ellipsometric measurements is represented by VUV domain, which denotes the spectroscopic range below 190 nm or energy above 6.5 eV. It was first applied at the BESSY synchrotron in Berlin [80] at photon energies up to 35 eV. Any transparent dielectric and wide band gap semiconductor is suitable for VUV ellipsometry, which comes with an increased sensitivity to film thickness and increased access to unique spectral features, like distinguishing between similar grown materials and correlating their mechanical, optical and electrical properties [81]. The importance of VUV ellipsometry consists in analyzing materials used in optoelectronics, high-power and high-temperature devices. There

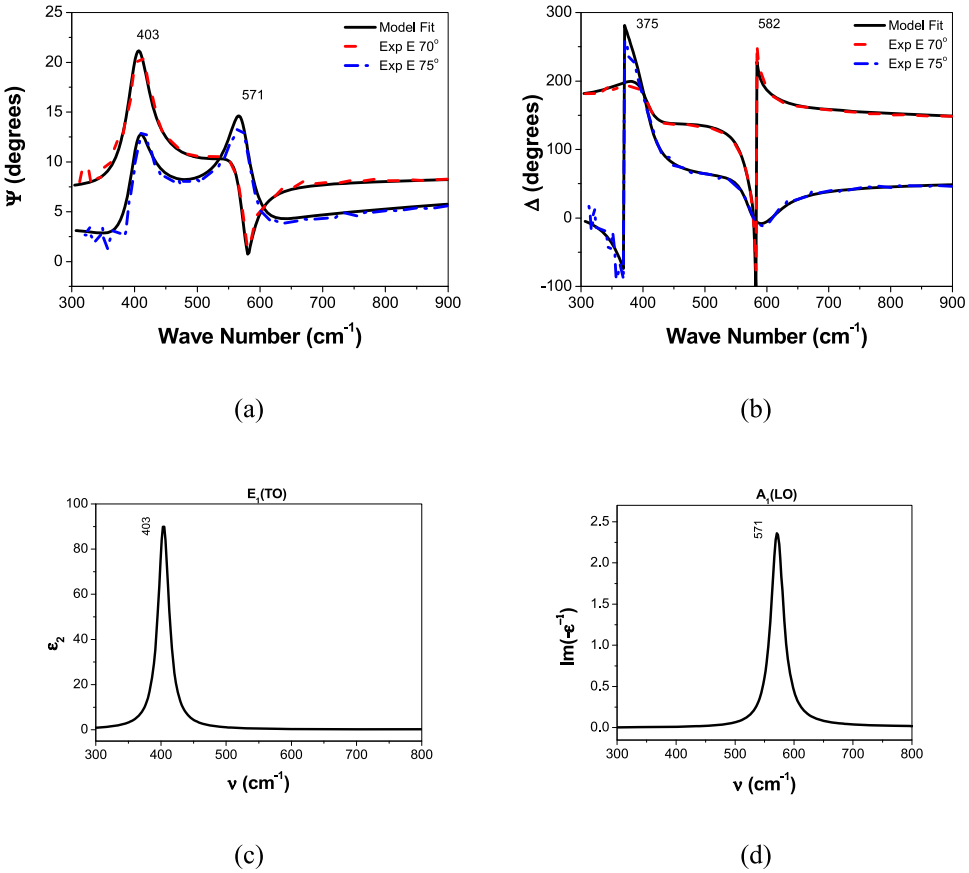

Fig. 10 a, b Experimental and simulated IR spectra of the Ψ and Δ ellipsometric parameters and (**c, d**) E_1(TO) and A_1(LO) frequency modes for ZnO:N film deposited by reactive sputtering in atmosphere with 10% N_2 and treated at 550 °C [Adapted from reference [76] with the permission of Elsevier]

are several deposition methods used to achieve thin films characterized by VUV ellipsometry, like PLD [82], sputtering [83], sol–gel combined [84], epitaxy [85], atomic layer deposition (ALD) [86]. VUV ellipsometry may be applied to lithography (157 nm), front end (*high-k* thin films) and back end (porous *low-k* interlayer dielectrics) processing. There is a continuous search in lithography industry to minimize the feature sizes, which led to the development of new materials, with new optical constants, making the lithography process a more feasible one [87]. Due to setup complexity and costs, commercial instruments do not allow measurement above 9.5 eV, and the number of VUV ellipsometers is still small. Consequently, the number of publications in this field is still small, most of them not dealing with sol–gel films. An example of applying VUV is the study of ZnO dielectric function, experimentally and theoretically obtained, in the 4.0–9.5 eV by Schmidt-Grund et al. [88]. The authors found for ZnO films deposited by PLD on Al_2O_3 substrate that the differences between both dielectric functions can be related to the strong excitonic contributions near the band gap. Also, it is known that Wurtzite-structure ZnO is optically uniaxial, and the authors found that the anisotropy is more pronounced in the theoretical dielectric function spectra. Other materials measured and characterized by VUV ellipsometry were SiC [89], GaN [90], AlN [91], AlGaN [92] and AlInN [93], due to the electronic transitions that occur at these photon energies, and due to possibility to differentiate between ordinary and extraordinary dielectric functions.

4.2 Infrared spectroscopic ellipsometry (IRSE)

The results of this chapter form the subject of a future paper (to be published).

Since IRSE technique (analysis) developed considerably, it is possible nowadays to have optical (dielectric) constants on a large spectral range from UV to Mid IR. To this end, we performed an ellipsometric study of ITO thin films deposited by sol–gel dip-coating method. The films, containing 15 layers were deposited on three different substrates: glass, SiO_2/glass and SiO_2/Si and analysed separately in the UV–vis–NIR (0.19–1.7 μm) and in the Mid IR (2–33 μm) spectral ranges.

Ellipsometric simulations were based on the general oscillator model (see the models in Fig. 11) which contains Tauc-Lorentz oscillators for UV spectral range and Gaussian and Drude for IR range (see definition of the models in Section 1.2) in both cases. The ellipsometric parameters Ψ and Δ (experimentally measured and computed with the models shown in the first row), the film thickness and the optical constants (obtained from the best fit), together with the Mean Squared Error (MSE) are presented in Fig. 11 for the range 0.35–33 μm (0.03–3.5 eV).

The transition between the spectral regions of the two ellipsometers (from 1700 nm alias 0.72 eV) is hardly noticeable in the data, indicating a good agreement between these two separately fitted regions.

The vibrational bands of ITO films were obtained directly by IRSE (300–1400 cm^{-1}) spectra of Ψ and Δ (Fig. 12 and Table 3).

The Infrared spectra of the ITO thin films reveal the presence of vibrational bands which were attributed to In–O–In, In–OH, Si–OH, and Si–O–Si, respectively [94–99]. The observed infrared modes are in good agreement with the vibrational bands from literature.

5 Complex features of ellipsometric analysis

5.1 Porosity and porosimetry

5.1.1 Porosity

It is well known that by sol–gel method pores are easily achieved in the thin film structure. Duta et al. [69]. showed that the ITO films obtained by sol–gel have a porosity of 11–19% in comparison with the ITO films prepared by sputtering (2–10%). The values of porosity were calculated from ellipsometry, knowing the refractive index, as it is shown in the following equation:

$$P = 1 - \frac{n^2 - 1}{n_d^2 - 1} \times 100(\%) \tag{13}$$

where n is the refractive index of current material and n_d-the refractive index of the material without pores.

Generally, there are two kinds of porosities in the films: intrinsic and extrinsic. The intrinsic one is related to the preparation method and is formed by small micropores (< 2 nm) of similar size as crystallite size (~10 nm). One suitable example is of TiO_2 sol–gel film doped with PEG [100]. This film has an intrinsic porosity due to the preparation method and doping with PEG (polyethylene glycol) leads to an extrinsic one, where the pore size is determined by PEG molecular weight. The extrinsic porosity is very significant after the first layer deposition.

SE measurements have shown that the total porosity (intrinsic and extrinsic) has similar values for all doped films after the deposition of a second layer, independent of the molecular weight of the PEG used, due to the densification of the films, that confines extrinsic porosity to the film outer surface. Cross-section SEM analysis of the films confirmed that in multilayer films extrinsic porosity remains located mostly at the outer layer of the film [101]. It was observed also that the pore size is influenced by the nature of the substrate, thus the pores are larger (50–200 nm) when

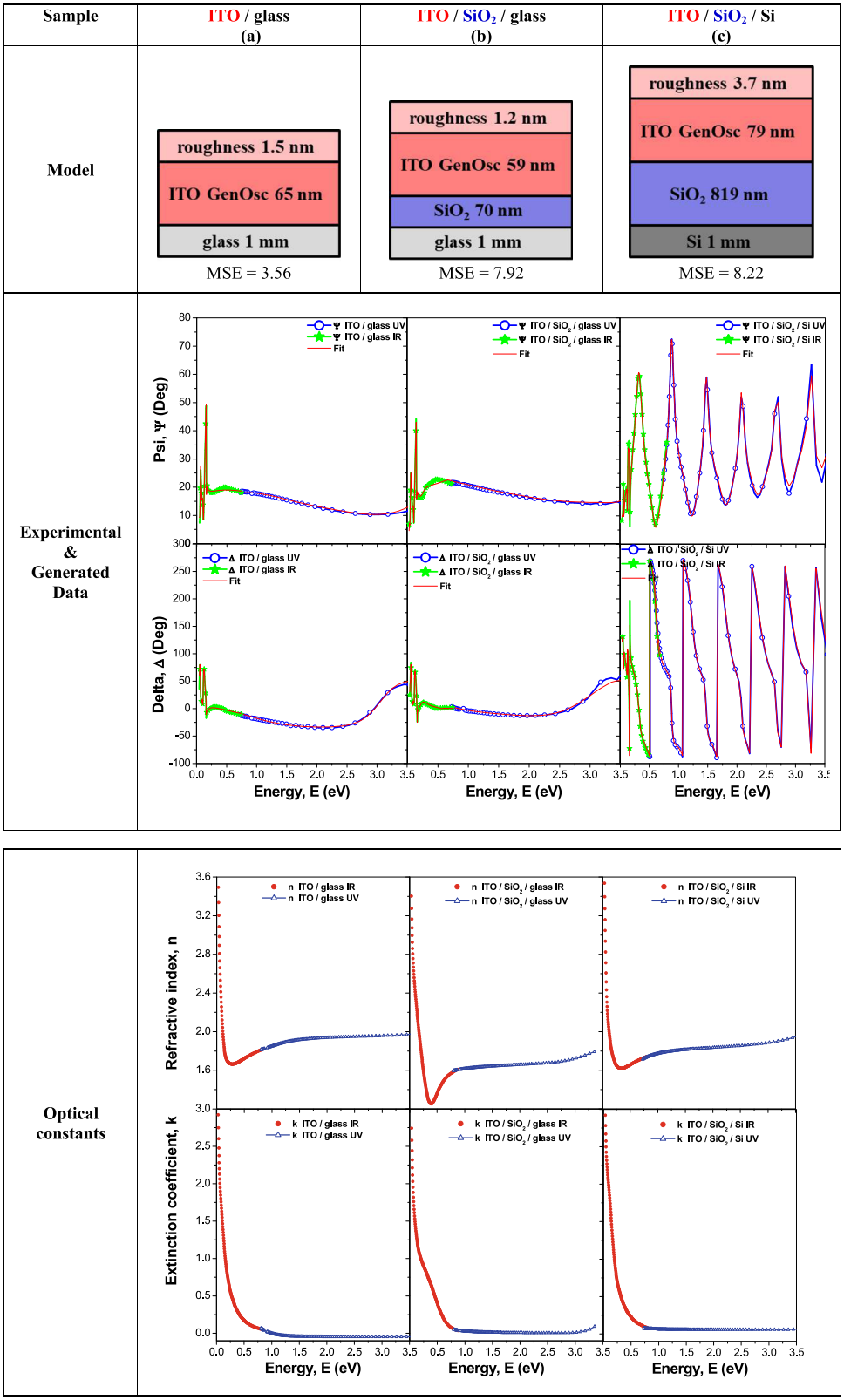

Fig. 11 Comparison between the optical properties of ITO sol–gel films deposited on: (**a**) glass, (**b**) SiO_2/glass and (**c**) SiO_2/Si

the films are deposited on FTO (Fluorine doped Tin Oxide coated glass) compared to glass (microscope standard slides) or silicon (below 20 nm) [102].

Some examples of porous films investigated by ellipsometry can be found in the application of mesoporous sol–gel silica thin film as vapor sensor in humid

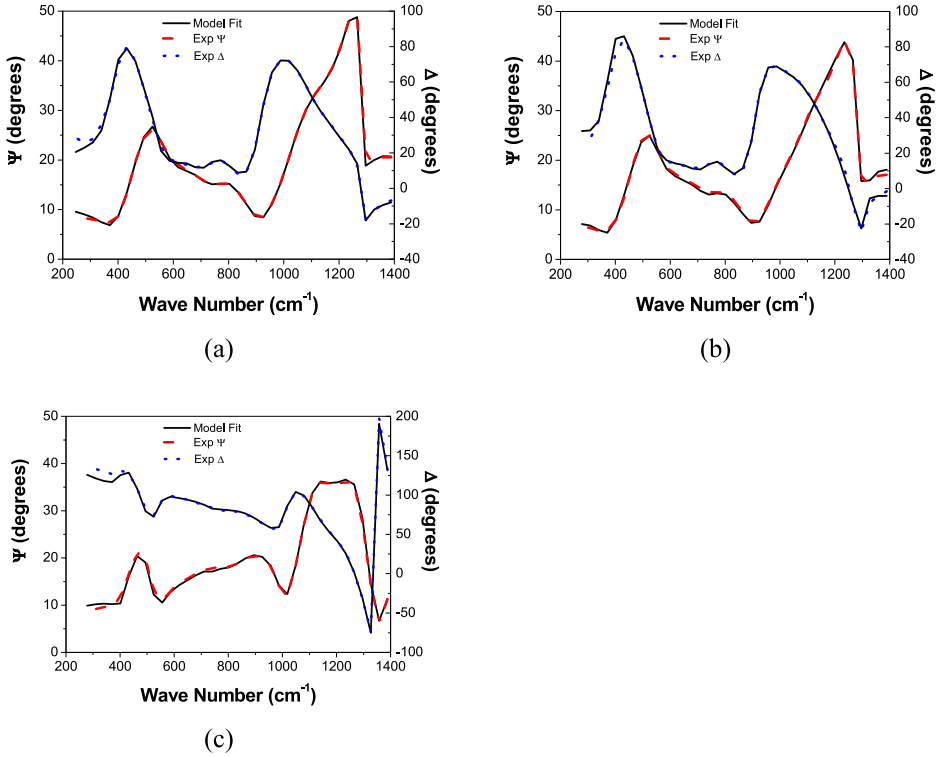

Fig. 12 Experimental and simulated Ψ and Δ spectra of ITO sol–gel films deposited on: (**a**) glass, (**b**) SiO_2/glass and (**c**) SiO_2/Si

Table 3 The vibrational bands of the ITO films from IRSE analysis and their assignation from literature

Substrate / Vibrational bands (cm^{-1})			Vibrational band from literature (cm^{-1})	Assignation of the chemical bands
Glass	SiO_2/ Glass	Si		
376	359	371	378 [94]	In–O
435	432	469	449, 476 [94, 95]	ITO
522	525	525	520 [96]	Si
610	–	585	564, 603 [95]	ITO
856	849	843	854 [97]	In–OH
919	893	909	880 [97]	Si–OH
997	987	1016	962 [97]	Si–OH
1107	–	1057	1070, 1110 [98, 99]	Si–O–Si
1236	1236	1236	1200-1260 [99]	Si–O–Si

environments [103], inorganic sol–gel films obtained from organic precursors (evaluated by SE and TEM showing small pore dimension and regular arrangement) [104], sol–gel polyfluoroalkyl-silica films with antireflection properties for photovoltaic application [105].

On the other hand usage of the Effective Medium Approximation (EMA) model (see Section 1.2) in ellipsometric spectra simulation is a direct and fast determination of the volume fractions of the film components and their porosity (void content). An example in this regard is the analysis of Er-doped SiO_2-TiO_2 binary system (used in planar optical waveguides). The films were deposited on oxidized silicon wafers by sol–gel dipping and spinning methods and annealed 30 min at 900 °C. By fitting the ellipsometric spectra with EMA model, the volume fractions of SiO_2, amorphous TiO_2, anatase, rutile, and voids were obtained [106]. In Table 4 are exemplified some papers related to the porosity calculations on the TiO_2 sol–gel films.

5.1.2 Porosimetry

The stringent necessity to find out the porosity of thin films led to the construction of an independent apparatus, Ellipsometric Porosimeter (EP), which is a device that couples the classic spectroscopic ellipsometer with an adsorption tool. An important feature of EP is the obtaining of the amount adsorbed during the experiment through the evolution of the optical properties of the porous material [114].

The uniqueness of the EP technique relies on its capacity to measure the porosity of extremely thin films, <10 nm, on its speed of measurement and reproducibility. It is well matched for extremely thin film pore size and pore distribution measurements, but the most fundamental feature of EP is to determine the open film porosity.

Löbmann highlighted the general features of the EP on TiO_2 [115] and TiO_2-MgF_2 [116] sol–gel films. In his review [117] he showed the possibility to evaluate open porosity, pore radius distribution and elastic properties in situ measurements. More than that, in this review the

Table 4 The time evolution of the papers involved in the porosity calculation of the sol–gel TiO_2 films by ellipsometry

Year of publication	Studied films	Highlights	Papers from literature
1997	Undoped TiO_2	It is the evidenced the dependence of pore volume by the water and solvent quantity in the preparation of the sol process.	[100]
2007	TiO_2:Au	The mass-transfer processes within the films were optimized by following the porosity changes during film synthesis.	[107]
2008	TiO_2:S	It is underlined the influence of the annealing temperature and deposited layers number on the porosity.	[108]
2011	TiO_2:Hg	It was correlated the change in porosity with the increase in the size of the grains, the density of the layers and/or pore destruction in films during increasing treatment temperature and number of dipping.	[109]
2014	TiO_2:PEG	The addition of PEG leads to an extrinsic porosity, where the pore size is determined by PEG molecular weight. It is shown the influence of the substrate on the film porosity.	[101, 102]
2015	TiO_2–P_2O_5	The dependence between pore size and proton conductivity—a new route in the design of highly proton conducting mesoporous inorganic thin-films.	[110]
2016	Nb-doped TiO_2	Controlling the sensitivity of the CO sensor by the film porosity.	[111]
2016	TiO_2:Al_2O_3	Open porosity variation of the film with dopant ratio. The film performances depend on the material composition rather than on the annealing temperature	[112]
2019	TiO_2	The adjustment of the porosity of Titania, by modifying the sol–gel fabrication process, to obtain the desired permeability for liquids and gases in sensing devices.	[113]

authors present a comparison between results obtained by EP and UV–vis Spectroscopy and SEM. The porosity depends on the sol–gel synthesis, number of depositions, thermal treatment and type of dopants. AZO thin films were deposited on borosilicate glass in coating-firing cycles (intermediary thermal treatment at 550 °C for 10 min after each layer deposition, followed by the final thermal treatment at 500 °C for 1 h in forming gas) [118] until the desired thickness is achieved. The authors showed that the porosity of a sol–gel Aluminum doped Zinc Oxide (AZO) film, with 90 - 125 nm thickness, containing 3 layers decreases from 14 to 5% after 7 depositions, arriving at 3% after 15-fold coating. The decrease in AZO porosity with the number of layers is related to the thermal treatment of the samples, during sol–gel synthesis.

Recently, Reid et al. [119] used EP in the study of the mesoporous inorganic thin films and Loizillon et al. [120], with the help of EP get advanced insights on the pores interconnectivity in the mesoporous silica.

The thickness and porosity both play an important role in the electrical (electrochemical) properties of thin films and/or substrates, which could be useful for a lot of applications, such as: gas and biosensor, solar cell, and so on [69, 114, 117].

5.2 Anisotropy

Anisotropy is defined as the characteristic of a material to exhibit variations in physical properties along different molecular axes. So, if we think about a material that exhibits different optical properties depending on the polarization direction of a light beam propagating through that material, then we can consider it o*ptically anisotropic*. Anisotropic samples were first characterized by ellipsometry in the 1970s with the development of generalized ellipsometry [121], and later, the anisotropy study was enhanced due to the development of a new 4×4 matrix method [122, 123] in the 1990s.

The optical properties of a material depend on the underlying atomic or molecular structure. In addition, in an anisotropic material the light traveling in different directions leads to different values for n and k (Fig. 13). This means that the propagation speed of light varies with the oscillating direction of the electric field, as a result of the refractive index variation. According to these refractive indices, anisotropic materials are classified into two categories, i.e., *uniaxial* with two different optical properties ($n_x = n_y \neq n_z$), and *biaxial* with three different optical constants ($n_x \neq n_y \neq n_z$), respectively.

An important cause of *uniaxial properties* in sol–gel films is the in-plane tensile stress [125]. The stresses will influence the film microstructure during drying and sintering processes, which in the end will cause the mechanical failure of the films. This makes difficult to achieve the desired thickness of single sol–gel coating for inorganic films.

Birefringence is a measure of optical anisotropy, defined as the maximum algebraic difference between two refractive indices measured in two perpendicular directions. If we consider a birefringent material, then the incident light splits

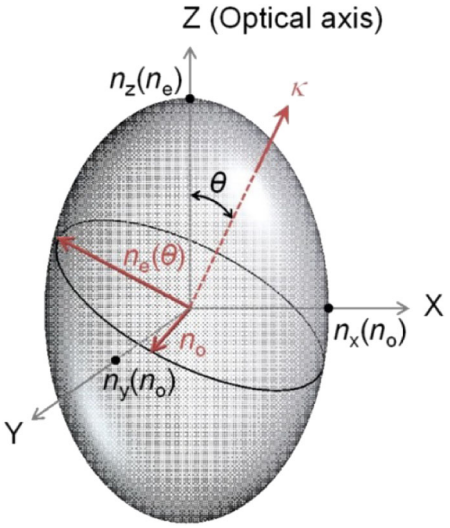

Fig. 13 Schematic view of the refractive index ellipsoid for a uniaxial material [124]

into two beams as it travels through the material. The propagation speed is constant when the oscillating direction is perpendicular to the optical axis and such light beam is called the *ordinary ray*, which experiences constant refractive index n_o. But the light beam whose oscillatory direction is parallel to the optical axis and its speed varies with the direction is called the *extraordinary ray* and experience refractive index n_e that varies with the direction of propagation of the light.

Examples of anisotropic materials consist of crystalline materials with tetragonal (rutile), hexagonal (sapphire), rhombohedral ($BiFeO_3$) orientations, crystalline organic chains, liquid crystals, sugars, materials that may be strained during processing, like PET sheets and spin-on films and materials with preferred orientation growth, especially columnar films. Anisotropic thin films are used in devices that rely on the manipulation of polarized lights, like liquid crystal displays, beam splitters, wave plate designs, just to name a few. Therefore, an improvement of the birefringence is desirable. We find such an example in the study of Xiao et al. [126]. on SiO_2 thin films. They found that the as-deposited SiO_2 thin films are porous with a tilted-columnar structure and low refractive index. By infiltrating ZrO_2 into SiO_2 columnar films, the linear birefringence is greatly enhanced. The transmission measurement results showed an increment in transmission difference (ΔT) of about ten times larger than that of as-deposited films.

Anisotropy can be *natural* or *induced* (for example by thickness-strain [127] or thermal treatment). One example of *natural anisotropy* is presented by Gartner et al.[128]. in the case of multilayer Fe_2O_3 *films*, deposited by the sol–gel method on glass substrate (Fig. 14).

The ellipsometric measurements showed that the birefringence values ($\Delta n = n_0 – n_e$) of the sol–gel films

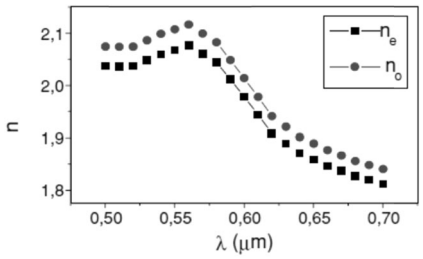

Fig. 14 The dispersion of ordinary (n_o) and extraordinary (n_e) refractive index of Fe_2O_3 film with two depositions and thermally treated 1 h at 300 °C [Reproduced from reference [128] with the permission of Springer]

(0.05–0.08) are smaller than the values of the α-Fe_2O_3 single crystal [129] (which are around 0.28), but increase with the crystallization of the films.

An *induced anisotropy* by the strain of different thickness and substrates of VO_2 sol–gel films was studied by Wan et al.[130].. They used in the ellipsometric fitting procedure of the film, grown on c-plane-oriented sapphire the anisotropic model because the sapphire in the mid- and far infrared presents a significant dispersion.

To study the growth kinetics of thin films during fabrication processes, both ex situ and in situ spectroscopic ellipsometry can take the anisotropy and the porosity of the films into account, as Laha et al. showed in the case of ZnO nanocrystalline layers [12]. They found that the asymmetric shape of the in situ curves, just as for the ex situ measurements, demonstrates the anisotropic nature of the layer, which in itself can be considered as a first indication of ZnO nanocrystal array growth.

Evtushenko et al. [131] reminded that TiO_2-based films may have anisotropy which can be used in many integrated optics applications. To this end they prepared sol–gel TiO_2 films and thermally treated them at different temperatures (350, 400, and 450 °C) to follow the crystallization process of the samples and the induction of anisotropy. They found by ellipsometric studies that optical anisotropy increases strongly, upon formation of anatase, yielding in-plane birefringence values that doubled from 0.11 to 0.22 in the case of TiO_2 thin films deposited at 60° and annealed at 400 °C. Raising the annealing temperature to 900 °C to form rutile, the thin film birefringence increased further, but also led to low optical transparency due to increased absorption and diffuse scattering.

Koziara et al. [132] studied spin-coated polymer films and found that water sorption reduces the internal stresses in such polymeric membranes, and, therefore, it reduces the optical anisotropy, which is strongly correlated with the density of the films. Also, a high concentration of the deposition solution may increase the optical anisotropy of the resulting films, associated with the preferred orientations in the in-plane direction of the polymer chains.

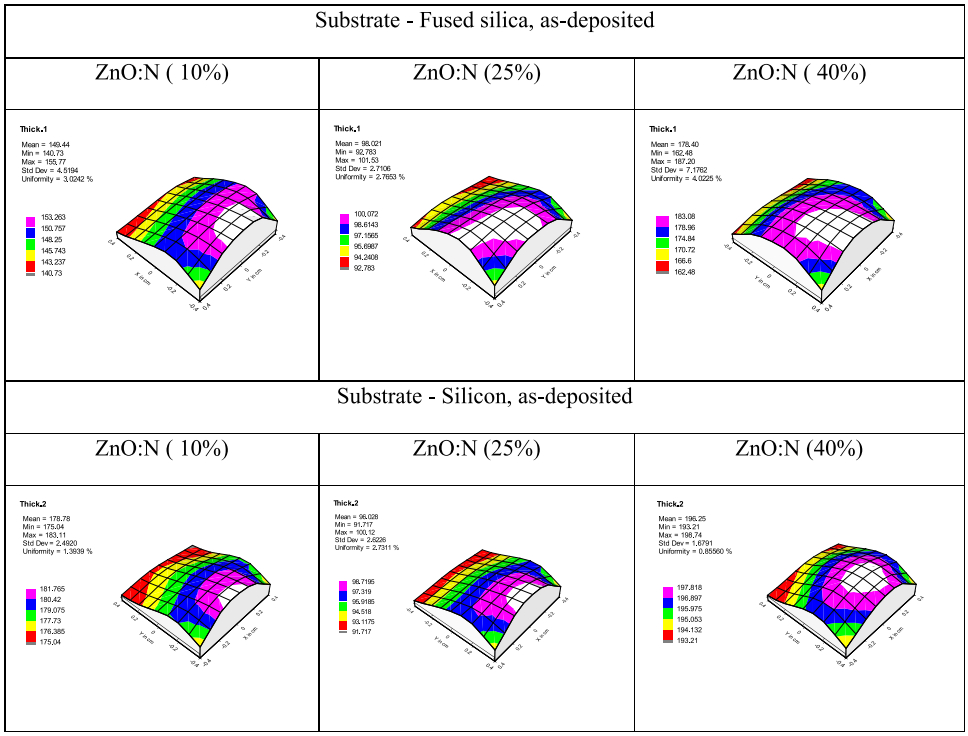

Fig. 15 Uniformity of ZnO:N as-deposited films on fused silica and silicon, resulted from ellipsometry mapping [Reproduced from reference [76] with the permission of Elsevier]

The emerging class of low-symmetry two-dimensional (2D) materials, crucial for creating diverse nanoscale devices, involves the study of the optical anisotropy, as one of the most fundamentally physical characteristic. The evaluation of anisotropic features of 2D materials requires a highly sensitive optical method and ellipsometry is one of them [133]. It is a very challenging approach due to the very small thickness of such materials and also the technological process of achieving 2D materials must be very pure.

Nowadays, spectroscopic ellipsometry is employed widely to study the anisotropic properties of insulators, semiconductors and organic materials [20] and provide exciting new challenges to ellipsometry researchers.

5.3 Mapping

For the characterization of thin films, the mapping technique is very useful in order to evaluate the uniformity of the sample thickness and/or optical distribution. The software uses a predetermined rectangular or circular model for scanning the surface and generates a thickness map. The spot size is 250 × 600 µm (on sample) and the data acquisition rate (per measurement spot, entire spectrum, in s): 0.3 (fastest), 1-2 (typical).

For example in the case of thin reactive sputtered ZnO films [76], the mapping analysis showed the influence of the substrate and the nitrogen amount (from the deposition atmosphere, which is a mixture of N_2, O_2, and Ar) on as-deposited film thickness (Fig. 15, Table 5). In this case the uniformity of thickness determined by ellipsometric mapping is around 90% for the sample deposited on fused silica and 96% for those deposited on silicon substrate [76].

Table 5 Maximum/minimum values of the layer thickness and of the uniformity for *as deposited* ZnO:N films on silicon and fused silica function of nitrogen content resulted from ellipsometric mapping

N_2 (%)	d_{film} (nm) deposited on Si	d_{film} (nm) deposited on Fused Silica
10	183.1/178.7	155.7/140.7
25	100.1/91.7	101.5/92.7
40	198.7/193.2	187.2/178.4

The mapping analysis was also used with good results in the last years on films prepared by sol–gel [134, 135], ALD [136–138] and Plasma Enhanced Chemical Vapor Deposition (PECVD) films [139, 140].

5.4 Bowing parameter

In general, the variation of band gap (Eg) in alloyed materials is a linear function of component concentration, respecting the Vegard's law:

$$Eg_{alloy} = (1 - x)Eg_A + xEg_B \quad (14)$$

where Eg_A, Eg_B, and Eg_{alloy} are the corresponding band gap of pure A, pure B, and of the alloy

x is the fraction of one ingredient in a composite A_xB_{1-x} material

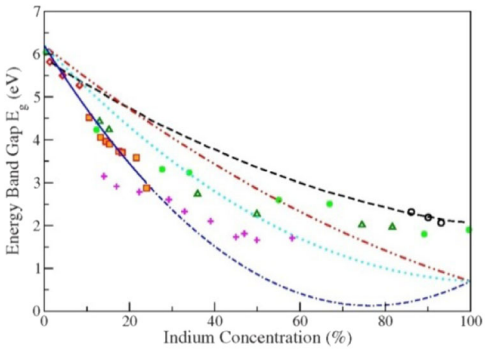

Fig. 16 Energy bandgap vs indium content: [141–148], [Adapted from reference [141] with the permission of AIP Publishing]

However, there are a lot of cases where the variation of Eg is not linear. In these cases, the Vegard's law is transformed in the parabolic equation:

$$Eg_{alloy} = (1-x)Eg_A + xEg_B - bx(1-x) \tag{15}$$

where b is denoted as "bowing parameter".

For example in the case of AlInN alloy [141], using this formula it was obtained $b = 10.36$, which is a valid value for pseudomorphically grown layers with an indium content between 13 and 24% only. A comparison with literature is shown in Fig. 16.

As can be seen in Fig. 16, in the case of AlInN alloy, but not only, the *Eg* values available in the literature vary significantly from publication to publication depending mainly on the deposition method. While Lukitsch et al. [149] report on samples grown by MBE, Peng et al. [143] and Guo et al. [144] used a sputtering technique. Samples grown by MOVPE were investigated by Yamaguchi et al. [145], Hums et al. [150]. and Kim et al. [146]. Theoretical calculations were performed by Goano et al. [147] as well as Wright and Nelson [151].

The bowing parameter concept was expanded from the films obtained by physical methods to the films deposited by chemical methods. It is known that the Eg value is a compositional and structural phase dependent parameter which varies with precursor concentration and aging conditions (time, temperature) and with dopant concentration for the doped films. Due to the fact that the design of the sol–gel film function of doping is one of the keys in obtaining a film with desired properties, we tabulated the papers from literature, which are dealing with this subject. Table 6 shows how the bowing parameter varies with the type and concentration of the dopant in the case of ZnO, TiO_2 and ITO sol–gel films in some of the recent papers [35, 152, 153].

In conclusion the Bowing parameter is a useful factor for predicting the content of dopant necessary to obtain a specific value for film bandgap.

The optical band gap is given by the following relation:

$$(\alpha h\nu)^n = A\left(h\nu - E_g\right) \tag{16}$$

where α is the absorption coefficient, $h\nu$ is the photon energy, A is a constant, E_g is the band gap and n denotes the type of transition ($n = 2$ for direct gap semiconductors) [165, 166] while the Urbach absorption tail is described by the following relation:

$$\alpha = \alpha_0 exp\left(\frac{h\nu}{E_u}\right) \tag{17}$$

where, α is the absorption coefficient, α_0 is a constant, $h\nu$ is the photon energy, and E_u is the Urbach energy.

The Urbach energy represents the width of the tail of localized states inside the band gap, which leads to absorption below the fundamental band gap. It is the largest in materials that are amorphous and have a large number of defects. As the defect density decreases, the Urbach energy should also decrease.

Miao et al. [156] studied the effect of Er doping and annealing on optical properties of ZnO sol–gel spin-coated thin films, deposited on a quartz substrate, and they found for the pure ZnO films a steep Urbach tail, while the films with 0.05 at.% of Er showed a slight broadening tail. A more broadening effect was observed for samples treated at 1000 °C. These effects might be due to alternation of band gap due to local strain or change of structure disorder and crystallinity and due to the non-homogeneous distribution of the minor impurities.

The doping effect on the Urbach energy was investigated also by Ali et al. [159]. In their work La and Sm doped ZnO films were deposited by spin coating on Si substrates, the concentration of La and Sm being varied between 0.2 and 5 wt%. They found that the optical bandgap of ZnO thin films shifts towards higher wavelengths (red shift) on incorporating La and Sm, due to their increased absorption ability for visible light, Sm doped films being more absorbing in the visible region as compared to La-doped ZnO films. This decreasing trend of E_g is due to the introduction of energy levels within the forbidden band just below the conduction band. By doping with La and Sm, high concentration of defects is introduced, which is responsible for the perturbation in band structure. These defects can be determined by Urbach relation. E_u dependence on the dopant concentration is opposite to that of E_g: higher E_u values indicate the higher concentration of defects, which creates more impurity levels within the forbidden gap, which leads to E_g decreasing. The red shift observed in this case suggests that the doped ZnO films may be used as visible light photocatalysts.

An opposite shifting effect (namely, a blue shift) was observed in the case of Er-doped ZnO films in the work of Chen et al. [167], due to the Burstein-Moss effect [168]. In

Table 6 Papers from literature related to Eg variation vs dopant concentration for sol–gel ZnO, TiO_2 and ITO films

Year of publication	Dopant concentration (%)	Eg variation	Literature
ZnO films			
2009	Mg (0–1)	$Eg(Mg_xZn_{1-x}O) = 3.333 + 1.1818x$	[154]
2013	Mn (0–0.2)	$Eg(Zn_{1-x}Mn_xO) = 3.176 + 1.924x$	[155]
2013	Er (0.5–3)	Eg(ZnO:Er) has a parabolic behavior with the increasing of the Er concentration.	[156]
2014	Cu (0–0.1)	*Eg* decrease from 3.43 to 3.22 eV.	[157]
2017	Mn (0-0.6)	$Eg(Zn1 - xMnxO) = -0.0331x + 3.1752$	[158]
2018	Fe (6–8)	Eg increases from 3.2 to 3.7 eV.	[38]
2019	La, Sm (0.2–10)	Eg has a decreasing trend with both dopant concentrations. A linear relationship between bandgap energy and *Urbach*[a] *energy* is established.	[159]
2020	Al (1.5–3)	Effect of concentration, aging, and annealing on band gap and Urbach energies is presented. Eg tends to decrease with increasing aging time for all Al concentrations.	[153]
TiO_2 films			
2008	Co (0–12)	Eg decreases when Co content increases.	[160]
2009	Fe (0–25)	Eg decreases when Fe^{3+} content increases.	[161]
2010	Fe (2–10)	$Eg(TiO_2 : Fe) = 3.43 - 0.41x$	[162]
ITO films			
2009	Zr (5,10,15)	Eg values retrieved from Ellipsometry (3.51–3.93 eV) were closer to the bulk indium oxide band gap value (3.6 eV) than that obtained from Kubelka–Munk method (2.63–3.06 eV).	[163]
2013	Co (1,3,5,8)	The optical band gap gradually decreases with improved cobalt concentration from 3.91 eV to 3.70 eV	[164]

[a]In order to understand the *Urbach* absorption, it is necessary to establish its relation with the band gap energy.

a semiconductor if we have some populated states closed to the conduction band, then this might lead to an increase in the band gap, as the absorption edge is pushed to higher energies; this phenomenon is known as Burstein-Moss effect. The effect occurs when the electron carrier concentration exceeds the conduction band edge density of states, which corresponds to degenerate doping in semiconductors, meaning that an electron from the top of the valence band can only be excited into conduction band above the Fermi level since all the states below the Fermi level are occupied states. Thus, the main observation in the work mentioned above, is that the optical band gap increases after Er doping and the blue shift of the band gap is due to the amorphous phase in the films.

Another example concerning the blue shift of the band edge is found in the work of Speaks et al. [153]. Al-doped ZnO and ZnO thin films were spin coated on glass substrates followed by annealing. The results showed that at higher concentration of sol gels, the obtained films aged more quickly and presented better properties, had larger grain sizes and the blue shift of the band edge became larger. As the grain size increases, the Urbach energy decreases, and the band gap of the doped ZnO films is higher that the un-doped films, thus a blue shift occurs. The annealing is necessary to obtain highly crystalline films, and it must be done above 450 °C for 1 h. Otherwise, low quality films are obtained, which will cause an increase in the band gap of ZnO, due to changes in crystallinity, in defect density or in tensile or compressive stress.

6 Prospects and drawbacks

A future challenge in ellipsometry is the further development of the available databases in order to cover the effects of composition, stress and defects, mainly in the topic of solar cells [169].

Also, future ellipsometric studies are expected to provide a greater understanding in important fields such as biology and medicine. A higher accuracy or extended wavelength ranges are necessary in these fields in order to overcome the difficulty represented by the similarity of visible-near UV spectra among organic materials [170].

In biological analysis, measurements at multiple angles of incidence are difficult to be performed in situ at the solid/

liquid interface due to the cellular limitations compared to the measurements in air, which can be considered a disadvantage of the ellipsometric method.

Moreover, the use of ellipsometry during heating/cooling process of a sample offers the possibility to study the dielectric properties of films during glass transition, as Hajduk et al. [171] showed for polymer films designed for organic optoelectronic devices. The advantage of this approach is to determine the temperature dependence of the thermal expansion coefficient and the spectral dependence of the thermo-optic coefficient, thus the ability to determine the thermal transition depth profiles, and to separate the reversible from irreversible processes. The drawback of the method consists of its complex modeling and time-consuming.

7 Summary

Our intention in this review was to prove that the spectroscopic ellipsometry is a versatile characterization technique for thin films, which can be used in a wide variety of applications. The following aspects were highlighted:

- basic knowledge of the appropriate models for fitting the experimental data, depending on the sample structure, composition, and appropriate application of the studied materials
- the *versatility* of the ellipsometry in the characterization of thin films
- the reliable results offered by SE in agreement with complementary methods, concerning film thickness and optical constants, as well as composition, structure and electrical parameters
- the *direct* information obtained from SE spectra, including visualization of different bands, estimation of film thickness, stability of the films and optical phonon contributions
- the spectral features of the films in *VUV and IR spectral ranges*. The possibility to obtain, for a certain film, the optical constants over a wide spectral domain
- the *porosity* evaluation by SE. Examples presented in this review illustrate the suitability of SE in determining extrinsic and intrinsic porosity of sol–gel thin films. The *porosimeter*, as a spin-off independent device starting from SE, was also mentioned
- the possibility of SE to offer information on the film *anisotropy*, which is a particularly challenging task for 2D materials, crucial for creating nanoscale devices
- the *surface mapping* over large areas, which can be extremely useful not only in the Si wafer manufacturing, but also in the evaluation of uniformity of some film parameters (thickness, optical constants)
- the *nonlinear variation of Eg* with different technological parameters (like dopants, precursor concentration and aging conditions) via the *bowing parameter* (the nonlinear term of Eg variation) in connection with these factors. Knowing the bowing parameter of each material is very helpful in the design of films with predetermined properties
- the evaluation of Urbach energy and its dependence on the optical band gap, a very useful approach in describing the phenomena in the adsorption region

As a general comment we can say that the correspondence between the results obtained by SE and other techniques is a very good one, highlighting the sensitivity and versatility of ellipsometry, a useful characterization technique in the field of sol–gel thin films.

Acknowledgements This paper was carried out within the research program "Science of Surfaces and Thin Layers" of the "Ilie Murgulescu" Institute of Physical Chemistry, financed by the Romanian Academy. The authors are grateful to Dr. L. Predoana for the sol–gel preparation of the ITO samples and to PhD student D. Mitrea for helping with the literature search. The financial support of the project M-ERA.NET 112/2019 within PNCDI III and EU (ERDF) and Romanian Government that allowed for the acquisition of the research infrastructure under POS-CCE O 2.2.1 project INFRANANOCHEM —No. 19/01.03.2009 are gratefully acknowledged.

Authors' contributions The authors read and approved the final manuscript.

Compliance with ethical standards

Conflict of interest The authors declare no competing interests.

References

1. Aspnes DE, Studna AA (1975) High precision scanning ellipsometer. Appl Opt 14:220–228
2. Muller RH, Farmer JC (1984) Fast, self-compensating spectral-scanning ellipsometer. Rev Sci Instrum 55:371–374
3. Kim Y-T, Collins RW, Vedam K (1990) Fast scanning spectroelectrochemical ellipsometry: In-situ characterization of gold oxide. Surf Sci 233:341–350
4. Aspnes DE (2014) Spectroscopic ellipsometry—Past, present, and future. Thin Solid Films 571:334–344
5. Röseler A, Korte E-H (2006) Infrared spectroscopic ellipsometry. In: Chalmers JM (ed) Handbook of Vibrational Spectroscopy. John Wiley & Sons, Ltd, Chichester, UK, p 1065–1090
6. Bruynooghe S, Bertin F, Chabli A et al. (1998) Infrared spectroscopic ellipsometry for residual water detection in annealed sol–gel thin layers. Thin Solid Films 313–314:722–726
7. Gartner M, Stanica N, Vass M (1990) Ellipsometric spectroscopy of pure oxygen and carbon monoxide covered copper films. Rev Roum Chim 35:713–720

8. Lazarescu V, Gartner M, Scurtu R et al. (2006) Fermi Level pinning at n-GaAs(110) electrodes. In: Marcus P, Maurice V (eds) Passivation of metals and semiconductors, and properties of thin oxide layers. Elsevier, Amsterdam, p 257–262
9. Hrabovsky D, Berini B, Fouchet A et al. (2016) Strontium titanate (100) surfaces monitoring by high temperature in situ ellipsometry. Appl Surf Sci 367:307–311
10. Kaspar TC, Reiser JT, Ryan JV, Wall NA (2018) Non-destructive characterization of corroded glass surfaces by spectroscopic ellipsometry. J Non Cryst Solids 481:260–266
11. Skopin EV, Deschanvres J-L, Renevier H (2020) In situ ellipsometry study of the early stage of ZnO atomic layer deposition on $In_{0.53}Ga_{0.47}As$. Phys Status Solidi 217:1900831
12. Laha P, Nazarkin MY, Volkova AV et al. (2015) In-situ ellipsometric characterization of the growth of porous anisotropic nanocrystalline ZnO layers. Appl Phys Lett 106:101904
13. Aryal P, Ibdah A-R, Pradhan P et al. (2016) Parameterized complex dielectric functions of $CuIn_{1-x}Ga_xSe_2$: applications in optical characterization of compositional non-uniformities and depth profiles in materials and solar cells. Prog Photovolt Res Appl 24:1200–1213
14. Trolier-McKinstry S, Chen J, Vedam K, Newnham RE (1995) In situ annealing studies of sol-gel ferroelectric thin films by spectroscopic ellipsometry. J Am Ceram Soc 78:1907–1913
15. Sengupta SS, Park SM, Payne DA, Allen LH (1998) Origins and evolution of stress development in sol-gel derived thin layers and multideposited coatings of lead titanate. J Appl Phys 83:2291–2296
16. Brinker CJ, Hurd AJ, Frye GC et al. (1990) Sol-gel thin film formation. J Non Cryst Solids 121:294–302
17. Hurd AJ, Brinker CJ (1988) Ellipsometric imaging of drying sol-gel films. MRS Proc 121:731–742
18. Hurd AJ, Brinker CJ (1988) Optical sol-gel coatings: ellipsometry of film formation. J Phys 49:1017–1025
19. Zudans I, Heineman WR, Seliskar CJ (2004) In situ dynamic measurements of sol−gel processed thin chemically selective PDMDAAC−silica films by spectroscopic ellipsometry. Chem Mater 16:3339–3347
20. Fujiwara H (2007) Spectroscopic ellipsometry: principles and applications. John Wiley & Sons, Ltd, West Sussex, England
21. Tompkins HG (2004) Industrial applications of spectroscopic ellipsometry. Thin Solid Films 455–456:772–778
22. Zollner S (2013) Spectroscopic ellipsometry for inline process control in the semiconductor industry. In: Ellipsometry at the Nanoscale. Springer Berlin Heidelberg, Berlin, Heidelberg, pp 607–627
23. Solano I, Parisse P, Cavalleri O et al. (2016) Investigating organic multilayers by spectroscopic ellipsometry: specific and non-specific interactions of polyhistidine with NTA self-assembled monolayers. Beilstein J Nanotechnol 7:544–553
24. Cobet C, Oppelt K, Hingerl K et al. (2018) Ellipsometric spectroelectrochemistry: an in situ insight in the doping of conjugated polymers. J Phys Chem C 122:24309–24320
25. Cody D, Babeva T, Madjarova V et al. (2020) In-situ ellipsometric study of the optical properties of LTL-doped thin film sensors for copper(II) ion detection. Coatings 10:423
26. Hilfiker JN, Pribil GK, Synowicki R et al. (2019) Spectroscopic ellipsometry characterization of multilayer optical coatings. Surf Coat Technol 357:114–121
27. Choi S, Kang C, Byun C-W et al. (2020) Thin-film transistor-driven vertically stacked full-color organic light-emitting diodes for high-resolution active-matrix displays. Nat Commun 11:1–9
28. Wang H, Madaan N, Bagley J et al. (2014) Spectroscopic ellipsometric modeling of a Bi–Te–Se write layer of an optical data storage device as guided by atomic force microscopy, scanning electron microscopy, and X-ray diffraction. Thin Solid Films 569:124–130
29. Hoffmann MA, Sharma A, Matthes P et al. (2020) Spectroscopic ellipsometry and magneto-optical Kerr effect spectroscopy study of thermally treated $Co_{60}Fe_{20}B_{20}$ thin films. J Phys Condens Matter 32:055702
30. Arwin H (2000) Ellipsometry on thin organic layers of biological interest: characterization and applications. Thin Solid Films 377–378:48–56
31. Mendoza-Galván A, Muñoz-Pineda E, Ribeiro SJL et al. (2018) Mueller matrix spectroscopic ellipsometry study of chiral nanocrystalline cellulose films. J Opt (U Kingd) 20:024001. (1–10)
32. Ostroff RM, Maul D, Bogart GR et al. (1998) Fixed polarizer ellipsometry for simple and sensitive detection of thin films generated by specific molecular interactions: applications in immunoassays and DNA sequence detection. Clin Chem 44:2031–2035
33. Khaleel MI, Chen Y-D, Chien C-H, Chang Y-C (2018) Microscopic imaging ellipsometry of submicron-scale bacterial cells. Trop J Pharm Res 16:2713
34. Lee SW, Lee SY, Choi G, Pahk HJ (2020) Co-axial spectroscopic snap-shot ellipsometry for real-time thickness measurements with a small spot size. Opt Express 28:25879
35. Aghgonbad MM, Sedghi H (2019) Spectroscopic ellipsometry studies on zinc oxide thin films deposited by sol-gel method with various precursor concentrations. Surf Rev Lett 26:1–9
36. Akhtar MS, Riaz S, Naseem S (2015) Optical properties of sol-gel deposited ZnS thin films: spectroscopic ellipsometry. Mater Today Proc 2:5497–5503
37. Noh M, Seo I, Park J et al. (2016) Spectroscopic ellipsometry investigation on the excimer laser annealed indium thin oxide sol–gel films. Curr Appl Phys 16:145–149
38. Aghgonbad MM, Sedghi H (2019) Optical and electronic analysis of pure and Fe-doped ZnO thin films using Spectroscopic Ellipsometry and Kramers-Kronig Method. Int J Nanosci 18:1–9
39. Losurdo M, Hingerl K (2013) Ellipsometry at the Nanoscale. Springer Berlin Heidelberg, Berlin, Heidelberg
40. Tompkins HG, McGahan WA (1999) Spectroscopic ellipsometry and reflectometry: a user's guide. Wiley, N.Y
41. Mia MNH, Pervez MF, Hossain MK et al. (2017) Influence of Mg content on tailoring optical bandgap of Mg-doped ZnO thin film prepared by sol-gel method. Results Phys 7:2683–2691
42. Aspnes DE (1982) Optical properties of thin films. Thin Solid Films 89:249–262
43. Bakkali H, Blanco E, Amrani M et al. (2018) An ellipsometric analysis to model the order-disorder transition in Au-SiO_2 nanogranular thin films induced by thermal annealing. Thin Solid Films 660:455–462
44. Jaglarz J, Dulian P, Karasiński P, Winkowski P (2020) Scattering phenomena in porous sol-gel-derived silica films. Coatings 10:509
45. Ramirez-Rincon JA, Gomez-Heredia CL, Corvisier A et al. (2018) Thermal hysteresis measurement of the VO_2 dielectric function for its metal-insulator transition by visible-IR ellipsometry. J Appl Phys 124:195102
46. Liu Y, Qiu J, Liu L (2018) Applicability of the effective medium approximation in the ellipsometry of randomly micro-rough solid surfaces. Opt Express 26:16560
47. Ngo D, Liu H, Sheth N et al. (2018) Spectroscopic ellipsometry study of thickness and porosity of the alteration layer formed on international simple glass surface in aqueous corrosion conditions. npj Mater Degrad 2:20
48. Kostruba A, Stetsyshyn Y, Mayevska S et al. (2018) Composition, thickness and properties of grafted copolymer brush

coatings determined by ellipsometry: calculation and prediction. Soft Matter 14:1016–1025
49. De Sousa Meneses D, Malki M, Echegut P (2006) Structure and lattice dynamics of binary lead silicate glasses investigated by infrared spectroscopy. J Non Cryst Solids 352:769–776
50. Jellison GE, Modine FA (1996) Parameterization of the optical functions of amorphous materials in the interband region. Appl Phys Lett 69:371–373
51. Johs B, Herzinger C, Dinan J et al. (1998) Development of a parametric optical constant model for $Hg_{1-x}Cd_xTe$ for control of composition by spectroscopic ellipsometry during MBE growth. Thin Solid Films 313–314:137–142
52. Wooten F (1972) Optical properties of solids. Academic Press, New York
53. Noh M, Seo I, Park J et al. (2016) Spectroscopic ellipsometry investigation on the excimer laser annealed indium thin oxide sol–gel films. Curr Appl Phys 16:145–149
54. Jellison GE (1993) Data analysis for spectroscopic ellipsometry. Thin Solid Films 234:416–422
55. Kim SY, Vedam K (1988) Simultaneous determination of dispersion relation and depth profile of thorium fluoride thin film by spectroscopic ellipsometry. Thin Solid Films 166:325–334
56. Adachi S (1999) Optical properties of crystalline and amorphous semiconductors. Springer, US, Boston, MA
57. J.A. Woollam Co. (2012) Guide to using WVASE spectroscopic ellipsometry data acquisition and analysis software. J. A. Woollam Co., Inc. Lincoln, NE USA
58. Schubert M, Tiwald TE, Herzinger CM (2000) Infrared dielectric anisotropy and phonon modes of sapphire. Phys Rev B 61:8187–8201
59. Aspnes DE (1980) Modulation spectroscopy/electric field effects on the dieletric function of semiconductors. In: Balkanski M (ed) Handbook on Semiconductors, Vol. 2. pp 125–127
60. Adachi S (1987) Model dielectric constants of GaP, GaAs, GaSb, InP, InAs, and InSb. Phys Rev B 35:7454–7463
61. Tanguy C (1995) Optical dispersion by Wannier excitons. Phys Rev Lett 75:4090–4093
62. Tompkins HG, Irene EA (2005) Handbook of ellipsometry. Norwich, NY
63. Grigorovici R, Stoica T, Vancu A (1982) Evaluation of the optical constants and thicknesses of weakly absorbing non-uniform thin films. Thin Solid Films 97:173–185
64. Stoica TF, Gartner M, Losurdo M et al. (2004) Spectro-ellipsometric study of the sol–gel nanocrystalline ITO multilayer films. Thin Solid Films 455–456:509–512
65. Covei M, Predoana L, Osiceanu P et al. (2016) Niobium/Vanadium doped TiO_2 multilayered sol-gel films: Structure, surface chemistry and optical properties. Ceram Int 42:13805–13811
66. Duta M, Simeonov S, Teodorescu V et al. (2016) Structural and electrical properties of Nb doped TiO_2 films prepared by the sol-gel layer-by-layer technique. Mater Res Bull 74:15–20
67. Zaharescu M, Teodorescu VS, Gartner M et al. (2008) Correlation between the method of preparation and the properties of the sol–gel HfO_2 thin films. J Non Cryst Solids 354:409–415
68. Parlog C, Gartner M, Osiceanu P et al. (1996) Optical and microstructural properties of $TiO_2(Ni^{2+})$ thin films. Ceram Int 22:95–99
69. Duta M, Anastasescu M, Calderon-Moreno JM et al. (2016) Sol–gel versus sputtering indium tin oxide films as transparent conducting oxide materials. J Mater Sci Mater Electron 27:4913–4922
70. Fujiwara H, Kondo M (2005) Effects of carrier concentration on the dielectric function of ZnO:Ga and In_2O_3:Sn studied by spectroscopic ellipsometry: Analysis of free-carrier and band-edge absorption. Phys Rev B 71:075109
71. Lin K, Wu S-W, Li L-Y, Sawada Y (2016) Spectroscopic ellipsometry study of the optoelectrical properties of In_2O_3:Sn-ZnO:Al thin films deposited through alternating sputtering. J Ceram Soc Jpn 124:528–531
72. Schubert M (2004) Infrared ellipsometry on semiconductor layer structures: phonons, plasmons and polaritons. Berlin
73. Ossikovski R, Drévillon B, Firon M (1995) Infrared ellipsometry study of the thickness-dependent vibration frequency shifts in silicon dioxide films. J Opt Soc Am A 12:1797
74. Michail G, Kambylafka V, Kortidis I et al. (2016) On the growth of transparent conductive oxide ternary alloys Zn–Ir–O (ZIRO) by the means of rf magnetron co-sputtering. Thin Solid Films 617:3–8
75. Stroescu H, Anastasescu M, Preda S et al. (2013) Influence of thermal treatment in N_2 atmosphere on chemical, microstructural and optical properties of indium tin oxide and nitrogen doped indium tin oxide rf-sputtered thin films. Thin Solid Films 541:121–126
76. Nicolescu M, Anastasescu M, Preda S et al. (2012) Influence of the substrate and nitrogen amount on the microstructural and optical properties of thin r.f.-sputtered ZnO films treated by rapid thermal annealing. Appl Surf Sci 261:815–823
77. Bundesmann C, Buiu O, Hall S, Schubert M (2007) Dielectric constants and phonon modes of amorphous hafnium aluminate deposited by metal organic chemical vapor deposition. Appl Phys Lett 91:121916
78. Ashkenov N, Mbenkum BN, Bundesmann C et al. (2003) Infrared dielectric functions and phonon modes of high-quality ZnO films. J Appl Phys 93:126–133
79. Kang TD, Lee GS, Lee HS et al. (2006) Infrared ellipsometric study on PZT thin films. J Korean Phys Soc 49:1604–1610
80. Barth J, Johnson RL, Cardona M (1998) Spectroscopic ellipsometry in the 6-35 eV region. In: Palik ED (ed) Handbook of optical constants of solids II. Academic Press, San Diego, CA
81. Edwards NV (2003) Status and prospects for VUV ellipsometry (applied to high k and low k materials). In: AIP conference proceedings. AIP, pp 723–737
82. Schmidt-Grund R, Schubert M, Rheinländer B et al. (2004) UV–VUV spectroscopic ellipsometry of ternary $M_{gx}Z_{n1-x}O$ ($0 \le x \le 0.53$) thin films. Thin Solid Films 455–456:500–504
83. Suchaneck G, Chvostová D, Kousal J et al. (2011) Vacuum-ultraviolet ellipsometry spectra and structural properties of Pb(Zr,Ti)O_3 films. Thin Solid Films 519:2885–2888
84. Chvostová D, Pajasová L, Železný V (2008) Optical properties of PZT thin films by spectroscopic ellipsometry and optical reflectivity. Phys status solidi c 5:1362–1365
85. Dorywalski K, Lemée N, Andriyevsky B et al. (2017) Optical properties of epitaxial $Na_{0.5}Bi_{0.5}TiO_3$ lead-free piezoelectric thin films: Ellipsometric and theoretical studies. Appl Surf Sci 421:367–372
86. Boher P, Defranoux C, Heinrich P et al. (2004) VUV spectroscopic ellipsometry applied to the characterization of high-k dielectrics. Mater Sci Eng B 109:64–68
87. Hilfiker NJ, Bungay CL, Synowicki RA et al. (2003) Progress in spectroscopic ellipsometry: Applications from vacuum ultraviolet to infrared. J Vac Sci Technol A Vac, Surf, Film 21:1103–1108
88. Schmidt-Grund R, Rheinländer B, Kaidashev EM et al. (2008) Vacuum ultraviolet dielectric function and band structure of ZnO. J Korean Phys Soc 53:88–93
89. Wagner T, Hilfiker JN, Tiwald TE et al. (2001) Materials characterization in the vacuum ultraviolet with variable angle spectroscopic ellipsometry. Phys status solidi 188:1553–1562
90. Peters S, Schmidtling T, Trepk T et al. (2000) In situ monitoring of GaN metal-organic vapor phase epitaxy by spectroscopic ellipsometry. J Appl Phys 88:4085–4090
91. Wethkamp T, Wilmers K, Cobet C et al. (1999) Dielectric function of hexagonal AlN films determined by spectroscopic ellipsometry in the vacuum-uv spectral range. Phys Rev B 59:1845–1849

92. Cobet C, Esser N, Zettler JT et al. (2001) Optical properties of wurtzite AlxGa1−xN (x<0.1) parallel and perpendicular to the c axis. Phys Rev B 64:165203
93. Kasic A, Schubert M, Rheinländer B et al. (2001) IR-VUV dielectric function of Al1−xInxN determined by spectroscopic ellipsometry. MRS Proc 639:G6.13
94. White WB, Keramidas VG (1972) Vibrational spectra of oxides with the C-type rare earth oxide structure. Spectrochim Acta Part. A Mol Spectrosc 28:501–509
95. Silva GM, Faria EH, de, Nassar EJ et al. (2012) Synthesis of indium tin oxide nanoparticles by a nonhydrolytic sol-gel method. Quim Nova 35:473–476
96. Zerdali M, Hamzaoui S, Teherani FH, Rogers D (2006) Growth of ZnO thin film on SiO_2/Si substrate by pulsed laser deposition and study of their physical properties. Mater Lett 60:504–508
97. de Campos B, Freiria G, Ciuff K et al. (2017) ITO obtained by spray pyrolysis and coating on glass substrate. J Braz Chem Soc 28:2412–2420
98. Shahrokh Abadi MH, Delbari A, Fakoor Z, Baedi J (2015) Effects of annealing temperature on infrared spectra of SiO_2 extracted from rice husk. J Ceram Sci Technol 6:41–45
99. Tian R, Seitz O, Li M et al. (2010) Infrared characterization of interfacial Si−O bond formation on silanized flat SiO_2/Si surfaces. Langmuir 26:4563–4566
100. Zaharescu M, Crisan M, Simionescu L et al. (1997) TiO_2-based porous materials obtained from gels, in different experimental conditions. J Sol-Gel Sci Technol 8:249–253
101. Calderon-Moreno JM, Preda S, Predoana L et al. (2014) Effect of polyethylene glycol on porous transparent TiO_2 films prepared by sol–gel method. Ceram Int 40:2209–2220
102. Anastasescu M, Teodorescu VS, Buiu O et al. (2014) Substrate impact on optical and microstructural properties of TiO_2–PEG sol–gel films. Ceram Int 40:11803–11811
103. Boudot M, Cattoni A, Grosso D, Faustini M (2017) Ethanol–water co-condensation into hydrophobic mesoporous thin films: example of a photonic ethanol vapor sensor in humid environment. J Sol-Gel Sci Technol 81:95–104
104. Brigo L, Faustini M, Pistore A et al. (2016) Porous inorganic thin films from bridged silsesquioxane sol–gel precursors. J Non Cryst Solids 432:399–405
105. Agustín-Sáenz C, Machado M, Tercjak A (2020) Polyfluoroalkyl-silica porous coatings with high antireflection properties and low surface free energy for glass in solar energy application. Appl Surf Sci 509:144864
106. Zaharescu M, Cristea D, Obreja P, et al. (2007) SiO_2-TiO_2 undoped or (Er^{3+}) doped thin layers for integrate optics prepared by sol-gel method. In: International semiconductor conference. IEEE, pp 215–218
107. Buso D, Pacifico J, Martucci A, Mulvaney P (2007) Gold-nanoparticle-doped TiO_2 semiconductor thin films: Optical characterization. Adv Funct Mater 17:347–354
108. Crişan M, Brăileanu A, Răileanu M et al. (2008) Sol–gel S-doped TiO_2 materials for environmental protection. J Non Cryst Solids 354:705–711
109. Mechiakh R, Ben Sedrine N, Chtourou R (2011) Sol–gel synthesis, characterization and optical properties of mercury-doped TiO_2 thin films deposited on ITO glass substrates. Appl Surf Sci 257:9103–9109
110. Mosa J, Aparicio M, Durán A, Castro Y (2015) Mesostructured HSO3 -functionalized TiO_2 -P_2O_5 sol-gel films prepared by evaporation induced self-assembly method with high proton conductivity. Electrochim Acta 173:215–222
111. Duta M, Predoana L, Calderon-Moreno JM et al. (2016) Nb-doped TiO_2 sol–gel films for CO sensing applications. Mater Sci Semicond Process 42:397–404
112. Müller K, Hegmann J, Jahn R, Löbmann P (2016) Adjustable refractive index of titania–alumina thin films prepared from soluble precursor powders. J Sol-Gel Sci Technol 77:69–77
113. Checcucci S, Bottein T, Gurioli M et al. (2019) Multifunctional metasurfaces based on direct nanoimprint of titania sol–gel coatings. Adv Opt Mater 7:1801406
114. Bourgeois A, Turcant Y, Walsh C, Defranoux C (2008) Ellipsometry porosimetry (EP): thin film porosimetry by coupling an adsorption setting with an optical measurement, highlights on additional adsorption results. Adsorption 14:457–465
115. Bockmeyer M, Herbig B, Löbmann P (2009) Microstructure of sol-gel derived TiO_2 thin films characterized by atmospheric ellipsometric porosimetry. Thin Solid Films 517:1596–1600
116. Bittner A, Schmitt A, Jahn R, Löbmann P (2012) Characterization of stacked sol-gel films: Comparison of results derived from scanning electron microscopy, UV-vis spectroscopy and ellipsometric porosimetry. Thin Solid Films 520:1880–1884
117. Löbmann P (2017) Characterization of sol–gel thin films by ellipsometric porosimetry. J Sol-Gel Sci Technol 84:2–15
118. Jahn R, Löbmann P (2013) Microstructure and performance of AZO thin films prepared by sol-gel processing. J Sol-Gel Sci Technol 66:120–125
119. Reid B, Taylor A, Alvarez-Fernandez A et al. (2019) Photocatalytic template removal by non-ozone-generating UV irradiation for the fabrication of well-defined mesoporous inorganic coatings. ACS Appl Mater Interfaces 11:19308–19314
120. Loizillon J, Baumgartner B, Sinturel C et al. (2019) In-depth study of coating multimodal porosity using ellipsometry porosimetry in desorption scanning mode. J Phys Chem C 123:23464–23479
121. Azzam RMA, Bashara NM (1972) Generalized ellipsometry for surfaces with directional preference: application to diffraction gratings. J Opt Soc Am 62:1521–1523
122. Schubert M, Woollam JA, Johs B et al. (1996) Extension of rotating-analyzer ellipsometry to generalized ellipsometry: determination of the dielectric function tensor from uniaxial TiO_2. J Opt Soc Am A 13:875–883
123. Schubert M (1998) Generalized ellipsometry and complex optical systems. Thin Solid Films 313–314:323–332
124. Shima H, Naganuma H, Okamur S (2013) Optical properties of multiferroic $BiFeO_3$ films. In: Materials science—advanced topics. InTech, pp 33–61
125. Yeatman E (2016) Ellipsometry of sol–gel films. In: Klein L, Aparicio M, Jitianu A (eds) Handbook of sol-gel science and technology. Springer International Publishing, Cham, pp 1–11
126. Xiao X, Dong G, Fan Z et al. (2009) A facile process to improve linear birefringence of SiO_2 thin films. J Phys D Appl Phys 42:165305
127. Huffman TJ, Xu P, Qazilbash MM et al. (2013) Anisotropic infrared response of vanadium dioxide microcrystals. Phys Rev B 87:115121
128. Gartner M, Crisan M, Jitianu A et al. (2003) Spectroellipsometric characterization of multilayer sol-gel Fe_2O_3 films. J Sol-Gel Sci Technol 26:745–748
129. Hashimoto T, Yoko T, Sakka S (1993) Third-order nonlinear optical susceptibility of α-Fe_2O_3 thin film prepared by the sol-gel method. J Ceram Soc Jpn 101:64–68
130. Wan C, Zhang Z, Woolf D et al. (2019) On the optical properties of thin-film vanadium dioxide from the visible to the far infrared. Ann Phys 531:1900188
131. Evtushenko YM, Romashkin SV, Trofimov NS, Chekhlova TK (2015) Optical properties of TiO_2 thin films. Phys Procedia 73:100–107
132. Koziara BT, Nijmeijer K, Benes NE (2015) Optical anisotropy, molecular orientations, and internal stresses in thin sulfonated poly(ether ether ketone) films. J Mater Sci 50:3031–3040

133. Adamson P (2018) Ellipsometry of anisotropic graphene-like two-dimensional materials on transparent substrates. Opt Quantum Electron 50:403
134. Blanco E, González-Leal JM, Ramírez-del Solar M (2015) Photocatalytic TiO_2 sol–gel thin films: Optical and morphological characterization. Sol Energy 122:11–23
135. Furchner A, Sun G, Ketelsen H et al. (2015) Fast IR laser mapping ellipsometry for the study of functional organic thin films. Analyst 140:1791–1797
136. Diware MS, Park K, Mun J et al. (2017) Characterization of wafer-scale MoS_2 and WSe_2 2D films by spectroscopic ellipsometry. Curr Appl Phys 17:1329–1334
137. Dobrzański LA, Szindler M, Szindler M et al. (2015) The impact of atomic layer deposition technological parameters on optical properties and morphology of Al_2O_3 thin films. Opt Appl 45:573–583
138. Dobrzański LA, Szindler M, Szindler MM (2015) Surface morphology and optical properties of Al_2O_3 thin films deposited by ALD method. Arch Mater Sci Eng 73:18–24
139. Nečas D, Vodák J, Ohlídal I et al. (2015) Simultaneous determination of dispersion model parameters and local thickness of thin films by imaging spectrophotometry. Appl Surf Sci 350:149–155
140. Nečas D, Ohlídal I, Franta D et al. (2014) Assessment of non-uniform thin films using spectroscopic ellipsometry and imaging spectroscopic reflectometry. Thin Solid Films 571:573–578
141. Aschenbrenner T, Dartsch H, Kruse C et al. (2010) Optical and structural characterization of AlInN layers for optoelectronic applications. J Appl Phys 108:063533
142. Lukitsch MJ, Danylyuk YV, Naik VM et al. (2001) Optical and electrical properties of $Al_{1-x}In_xN$ films grown by plasma source molecular-beam epitaxy. Appl Phys Lett 79:632–634
143. Peng T, Piprek J, Qiu G et al. (1997) Band gap bowing and refractive index spectra of polycrystalline $AlxIn_{1-x}N$ films deposited by sputtering. Appl Phys Lett 71:2439–2441
144. Guo Q, Yahata K, Tanaka T et al. (2003) Growth and characterization of reactive sputtered AlInN films Phys Status Solidi (c) 0:2533–2536
145. Yamaguchi S, Kariya M, Nitta S et al. (1998) Observation of photoluminescence from $Al_{1-x}In_xN$ heteroepitaxial films grown by metalorganic vapor phase epitaxy. Appl Phys Lett 73:830–831
146. Kim KS, Saxler A, Kung P et al. (1997) Determination of the band-gap energy of $Al_{1-x}In_xN$ grown by metal–organic chemical-vapor deposition. Appl Phys Lett 71:800–802
147. Goano M, Bellotti E, Ghillino E et al. (2000) Band structure nonlocal pseudopotential calculation of the III-nitride wurtzite phase materials system. Part II. Ternary alloys $Al_xGa_{1-x}N$, $In_xGa_{1-x}N$, and $In_xAl_{1-x}N$. J Appl Phys 88:6476–6482
148. Wu J (2009) When group-III nitrides go infrared: new properties and perspectives. J Appl Phys 106:011101
149. Lukitsch MJ, Danylyuk YV, Naik VM et al. (2001) Optical and electrical properties of $Al_{1-x}In_xN$ films grown by plasma source molecular-beam epitaxy. Appl Phys Lett 79:632–634
150. Hums C, Bläsing J, Dadgar A et al. (2007) Metal-organic vapor phase epitaxy and properties of AlInN in the whole compositional range. Appl Phys Lett 90:22105
151. Wright AF, Nelson JS (1995) First-principles calculations for zinc-blende AlInN alloys. Appl Phys Lett 66:3465–3467
152. Amari R, Mahroug A, Boukhari A et al. (2017) Structural, optical and luminescence properties of ZnO thin films prepared by sol-gel spin-coating method: effect of precursor concentration. Chinese Phys Lett 35:016801
153. Speaks DT (2020) Effect of concentration, aging, and annealing on sol gel ZnO and Al-doped ZnO thin films. Int J Mech Mater Eng 15:2
154. Yang S, Liu Y, Zhang Y, Mo D (2009) Spectroscopic ellipsometry studies of Mg-doped ZnO thin films prepared by the sol-gel method. Phys Status Solidi Appl Mater Sci 206:1488–1493
155. Shaaban ER, El-Hagary M, Emam-Ismail M et al. (2013) Spectroscopic ellipsometry and magneto-transport investigations of Mn-doped ZnO nanocrystalline films deposited by a non-vacuum sol–gel spin-coating method. Mater Sci Eng B 178:183–189
156. Miao L, Tanemura S, Zhao L et al. (2013) Ellipsometric studies of optical properties of Er-doped ZnO thin films synthesized by sol–gel method. Thin Solid Films 543:125–129
157. Yang S, Zhang Y, Mo D (2014) Spectroscopic ellipsometry studies of sol-gel-derived Cu-doped ZnO thin films. Thin Solid Films 571:605–608
158. Masih VG, Srivastava A (2017) Redshift in the UV emission and curtailment in optical band gap of Manganese doped Zinc oxide thin films. J Mater Sci Mater Electron 28:8238–8245
159. Ali D, Butt MZ, Muneer I et al. (2019) Synthesis and characterization of sol-gel derived La and Sm doped ZnO thin films: A solar light photo catalyst for methylene blue. Thin Solid Films 679:86–98
160. Subramanian M, Vijayalakshmi S, Venkataraj S, Jayavel R (2008) Effect of cobalt doping on the structural and optical properties of TiO_2 films prepared by sol-gel process. Thin Solid Films 516:3776–3782
161. Wang MC, Lin HJ, Yang TS (2009) Characteristics and optical properties of iron ion (Fe^{3+})-doped titanium oxide thin films prepared by a sol-gel spin coating. J Alloy Compd 473:394–400
162. Zhang JZ, Shen YD, Li YW et al. (2010) Composition dependence of microstructure, phonon modes, and optical properties in rutile TiO_2: Fe nanocrystalline films prepared by a nonhydrolytic sol-gel route. J Phys Chem C 114:15157–15164
163. Jana S, Biswas PK (2009) Effect of Zr(IV) doping on the optical properties of sol-gel based nanostructured indium oxide films on glass. Mater Chem Phys 117:511–516
164. Mazloom J, Ghodsi FE (2013) Spectroscopic, microscopic, and electrical characterization of nanostructured SnO_2:Co thin films prepared by sol–gel spin coating technique. Mater Res Bull 48:1468–1476
165. Tauc J, Grigorovici R, Vancu A (1966) Optical properties and electronic structure of amorphous germanium. Phys status solidi 15:627–637
166. Ben Wannes H, Zaghouani RB, Ouertani R et al. (2018) Study of the stabilizer influence on the structural and optical properties of sol-gel spin coated zinc oxide films. Mater Sci Semicond Process 74:80–87
167. Chen Y, Xu XL, Zhang GH et al. (2010) Blue shift of optical band gap in Er-doped ZnO thin films deposited by direct current reactive magnetron sputtering technique. Phys E Low-dimensional Syst Nanostruct 42:1713–1716
168. Grundmann M (2006) The physics of semiconductors. Springer-Verlag, Berlin Heidelberg New York
169. Fujiwara H, Collins RW (2018) Spectroscopic ellipsometry for photovoltaics, Volume 1: Fundamental Principles and Solar Cell Characterization. Springer
170. Aspnes DE (2013) Spectroscopic ellipsometry—A perspective. J Vac Sci Technol A Vac, Surf, Film 31(058502):1–14
171. Hajduk B, Bednarski H, Trzebicka B (2020) Temperature-dependent spectroscopic ellipsometry of thin polymer films. J Phys Chem B 124:3229–3251